FEB 10 2000

0830-L-02 NAS 1.29/3-2:00-02

NASA Tech Briefs

National Aeronautics and
Space Administration

Electronic Components and Circuits

Electronic Systems

Physical Sciences

Materials

Computer Programs

Mechanics

Machinery

Fabrication Technology

Mathematics and Information Sciences

Life Sciences

2000-010923/NF C

INTRODUCTION

Tech Briefs are short announcements of innovations originating from research and development activities of the National Aeronautics and Space Administration. They emphasize information considered likely to be transferable across industrial, regional, or disciplinary lines and are issued to encourage commercial application.

Availability of NASA Tech Briefs and TSPs

Requests for individual Tech Briefs or for Technical Support Packages (TSPs) announced herein should be addressed to

National Technology Transfer Center
Telephone No. **(800) 678-6882** or via World Wide Web at **www2.nttc.edu/leads/**

Please reference the control numbers appearing at the end of each Tech Brief. Information on NASA's Commercial Technology Team, its documents, and services is also available at the same facility or on the World Wide Web at **www.nctn.hq.nasa.gov**.

Commercial Technology Offices and Patent Counsels are located at NASA field centers to provide technology-transfer access to industrial users. Inquiries can be made by contacting NASA field centers and program offices listed below.

NASA Field Centers and Program Offices

Ames Research Center
Carolina Blake
(650) 604-0893 or
cblake@mail.arc.nasa.gov

Dryden Flight Research Center
Lee Duke
(805) 258-3802 or
lee.duke@dfrc.nasa.gov

Goddard Space Flight Center
George Alcorn
(301) 286-5810 or
galcorn@gsfc.nasa.gov

Jet Propulsion Laboratory
Merle McKenzie
(818) 354-2577 or
merle.mckenzie@comail.jpl.nasa.gov

Johnson Space Center
Hank Davis
(281) 483-0474 or
hdavis@gp101.jsc.nasa.gov

John F. Kennedy Space Center
Gale Allen
(407) 867-6800 or
galeallen-1@ksc.nasa.gov

Langley Research Center
Dr. Joseph S. Heyman
(804) 864-6006 or
j.s.heyman@larc.nasa.gov

Glenn Research Center
Larry Viterna
(216) 433-3484 or
cto@lerc.nasa.gov

George C. Marshall Space Flight Center
Sally Little
(256) 544-4266 or
sally.little@msfc.nasa.gov

John C. Stennis Space Center
Kirk Sharp
(228) 688-1929 or
ksharp@ssc.nasa.gov

NASA Program Offices
At NASA Headquarters there are seven major program offices that develop and oversee technology projects of potential interest to industry:

Carl Ray
Small Business Innovation Research Program (SBIR) & Small Business Technology Transfer Program (STTR)
(202) 358-4652 or
cray@mail.hq.nasa.gov

Dr. Robert Norwood
Office of Aeronautics and Space Transportation Technology (Code R)
(202) 358-2320 or
rnorwood@mail.hq.nasa.gov

John Mulcahy
Office of Space Flight (Code MP)
(202) 358-1401 or
jmulcahy@mail.hq.nasa.gov

Gerald Johnson
Office of Aeronautics (Code R)
(202) 358-4711 or
g_johnson@aeromail.hq.nasa.gov

Bill Smith
Office of Space Science (Code S)
(202) 358-2473 or
wsmith@sm.ms.ossa.hq.nasa.gov

Roger Crouch
Office of Microgravity Science Applications (Code U)
(202) 358-0689 or
rcrouch@hq.nasa.gov

Granville Paules
Office of Mission to Planet Earth (Code Y)
(202) 358-0706 or
gpaules@mtpe.hq.nasa.gov

NASA Tech Briefs

February 2000
00-02

National Aeronautics and Space Administration

5 Electronic Components and Circuits

13 Electronic Systems

23 Physical Sciences

33 Materials

37 Computer Programs

41 Mechanics

45 Machinery

51 Mathematics and Information Sciences

55 Life Sciences

This document was prepared under the sponsorship of the National Aeronautics and Space Administration. Neither the United States Government nor any person acting on behalf of the United States Government assumes any liability resulting from the use of the information contained in this document, or warrants that such use will be free from privately owned rights.

4

BLANK PAGE

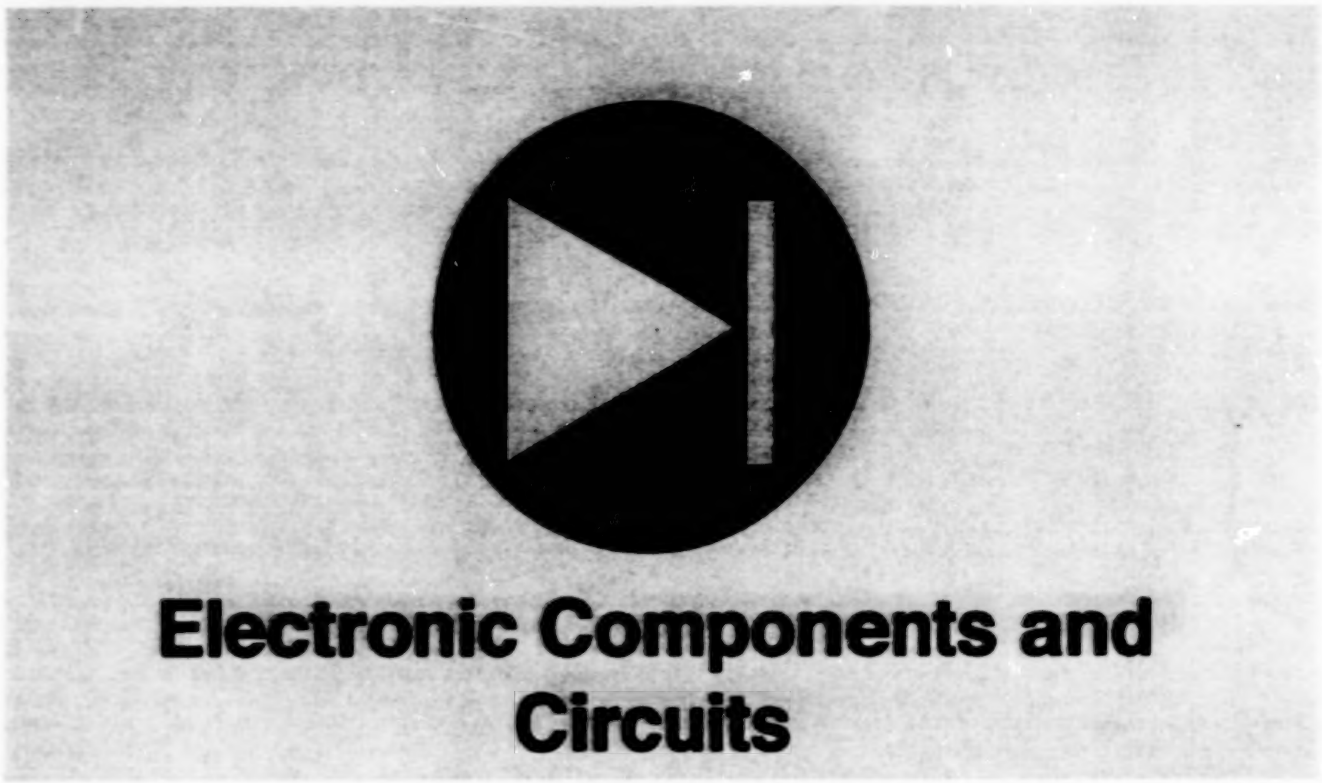

Electronic Components and Circuits

Hardware, Techniques, and Processes

7 Low-Sidelobe Phased-Array-Fed Cylindrical-Reflector Antenna
8 Electronic Modules With a 3-D Interconnection Scheme
9 Two Approaches to Improvement of InGaAs/InAlAs/InP HEMTs
10 DRAM Circuit Tolerates Single-Event Upsets
10 Integrated Optical Voltage-Measuring Apparatus
10 Forward-Link/Simulator PCI Card
11 Special-Purpose Interface for Fast Writing on a Hard Disk

BLANK PAGE

Low-Sidelobe Phased-Array-Fed Cylindrical-Reflector Antenna

Sidelobes can be reduced by choosing a suitable superquadric projected aperture.

NASA's Jet Propulsion Laboratory, Pasadena, California

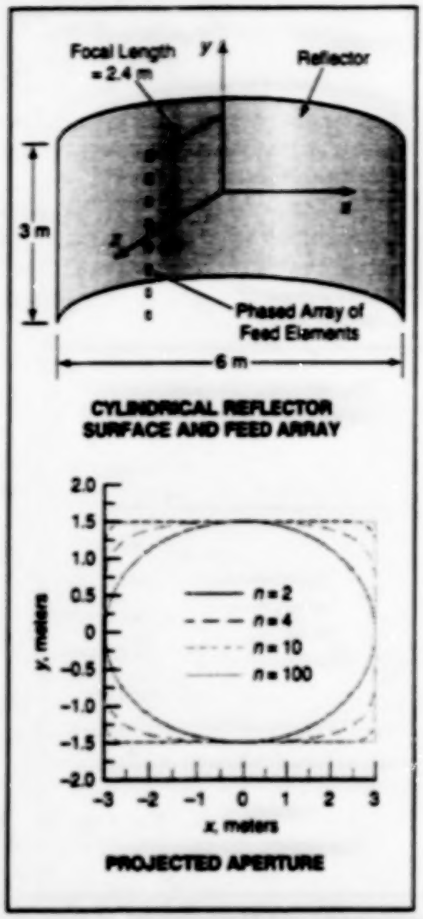

Figure 1. An Antenna With a Phased-Array Feed and a Parabolic Cylindrical Reflector can be used to reduce sidelobes at large scan angles with suitable choice of projected aperture-shaping parameter, *n*. The dimensions shown here are only for the numerical example described in the text; the dimensions specific to other applications could differ.

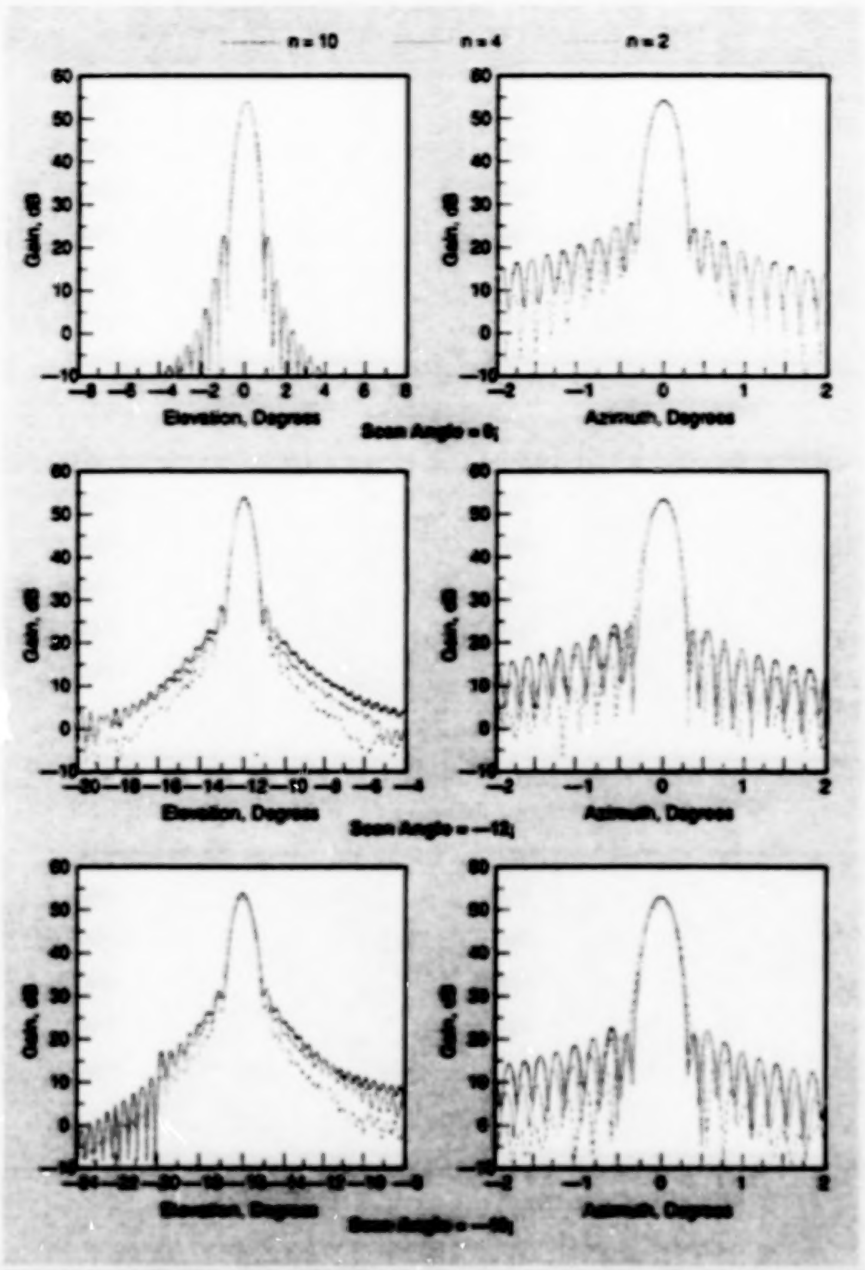

Figure 2. Some Results of Numerical Simulations are plotted for three different scan angles in the full-illumination case. In these plots, "elevation" signifies the far-field angle off the *z* axis in the *y,z* plane, and "azimuth" signifies the far-field angle off the *z* axis in the plane that includes *x* axis and the beam peak for the given scan angle.

A phased-array-fed cylindrical-reflector antenna with superquadric projected aperture has been designed to afford the ability to scan the beam over a wide angular range without having to resort to a large focal-to-diameter ratio and without incurring excessively strong sidelobes. The standard of comparison for this antenna is a paraboloidal-reflector antenna, which offers limited scanning capability at a low value of *F/D* (where *F* is focal length and *D* is diameter). The scanning capability of a paraboloidal-reflector antenna is improved by increasing *F/D*, but for a given large *D*, this entails an increase in *F* and thus in the size of the antenna structure needed to support a feed element at the focal point. The present phased-array-fed cylindrical-reflector antenna would be compact (*F/D* of only about 0.4, where the cross section of the cylindrical reflector, in *x–z* plane, is a parabola with diameter, *D*), yet would feature relatively low sidelobes at beam-scan angles as large as 16° off the geometric boresight axis in the plane that contains the cylindrical axis.

The basic antenna geometry (see Figure 1) is that of a parabolic cylindrical reflector. The cylindrical axis is the *y* axis, and the geometric boresight axis is the *z* axis. The phased array of feed elements lies on the focal line, which is parallel to the *y* axis, at a distance *F* from the apex of the parabola. The boundary of the reflector and thus of the aperture, as projected onto the *x,y* plane, is specified by the superquadric curve

$$\left|\frac{x}{a}\right|^n + \left|\frac{y}{b}\right|^n = 1;$$

where a and b are the lengths of the x and y semiaxes, respectively, of the aperture; and n is a parameter that can be chosen to control the rounded shape of the corners. The advantage of the superquadric projected aperture is that it is amenable to computational simulation of the performances of antennas with a variety of projected aperture sizes and shapes represented by various combinations of a, b, and n.

Computational simulations have been performed, following diffraction-analysis procedures based on a physical-optics formulation. The geometric parameters used in the simulations were $a = 3$ m, $b = 1.5$ m, $F = 2.4$ m, and three different values of n (2, 4, and 10). The feed elements were positioned at half-wavelength intervals (about 1.07 cm for a frequency of 14 GHz) along the focal line and were polarized along the y axis. The amplitudes of the array-feed excitations were tapered symmetrically about the central feed element, in proportion to $[\cos(\pi y/D_1)]^2$, where D_1 is the length of the array feed. The beam scan was realized through phase progression of the feeds.

For each value of n, two cases were considered. In one case, the reflector was under-illuminated: 233 feed elements were disposed symmetrically along the focal line from $y = -1.25$ to $y = 1.25$ m. In the other case, the reflector was fully illuminated: 281 feed elements were symmetrically disposed along the focal line for the full length of the cylindrical axis from $y = -1.5$ to $y = 1.5$ m.

The results of the computational simulation showed, among other things, that for a given beam scan off the z axis in elevation, the sidelobes are higher in the full-illumination than in the under-illumination case. The results also showed that the sidelobe levels for a given beam scan can be monotonically reduced at far angle from the peak of the beam by suitable choice of n, and the impact of the shaping parameter, n, on the sidelobe levels is more pronounced as the beam is scanned away from the boresight axis of the antenna (see Figure 2).

This work was done by Ziad Hussein and Eastwood Im of Caltech for **NASA's Jet Propulsion Laboratory**. *Further information is contained in a TSP [see page 1].*

NPO-20494

Electronic Modules With a 3-D Interconnection Scheme

Features would include versatility for expansion, testing, and integration.

NASA's Jet Propulsion Laboratory, Pasadena, California

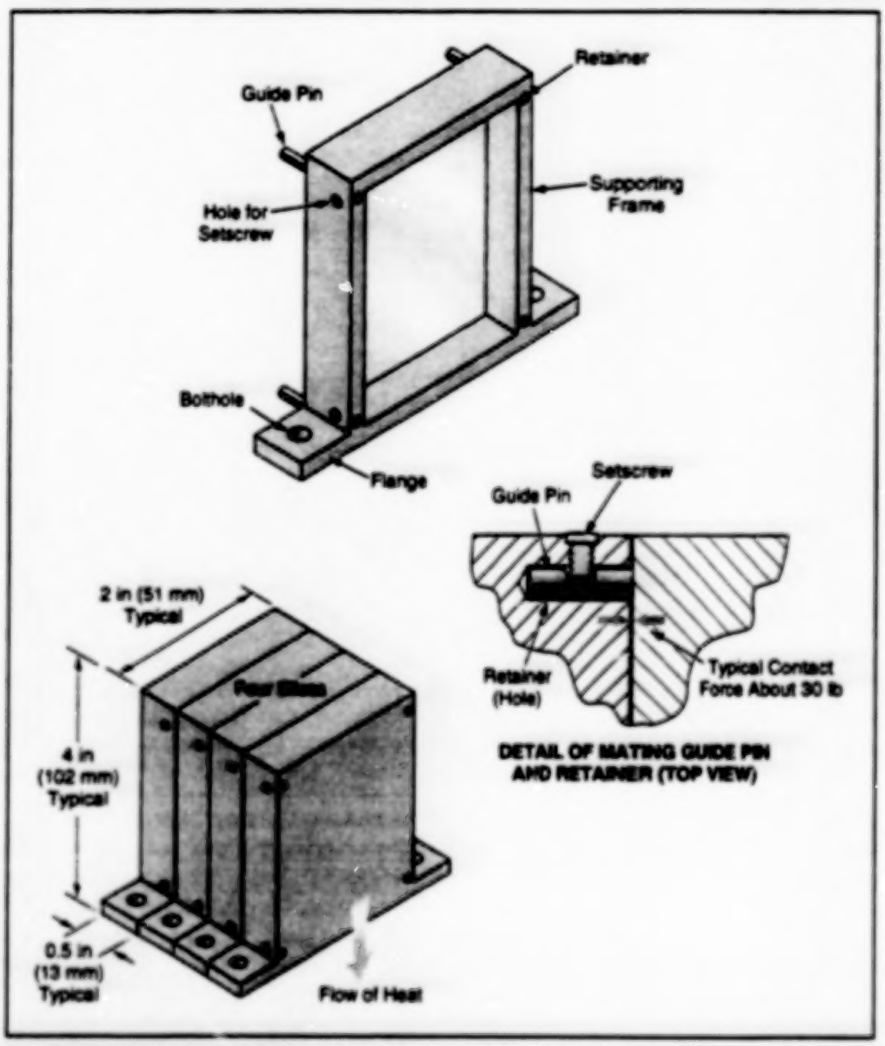

This Three-Dimensional Scheme for modular packaging and interconnection of electronic circuits offers electrical, thermal, and mechanical advantages over an older three-dimensional scheme.

An improved three-dimensional (3-D) scheme for modular packaging and interconnection of electronic circuits has been proposed to overcome deficiencies of an older scheme and to obtain additional advantages. In particular:

- The older scheme includes elastomer-based interconnections that fail at temperatures below –53 °C. The interconnections in the proposed scheme could function at temperatures from cryogenic to 200 °C.
- In the older scheme, it is necessary to disassemble an entire module in order to insert or remove individual submodules called "slices." In the proposed scheme, individual slices could be inserted or removed without disassembly of an entire module.
- The proposed scheme provides for better thermal management.
- In the older scheme, the capability for expansion is limited. The proposed scheme would provide versatility for integration of modules into systems, for integration of systems with each other, for expanding systems, and for configuring systems for testing.

An essential part of the scheme is to construct an electronic system with a common modular design for all subsystems. The figure illustrates selected aspects of the proposed scheme as applied to a four-slice module. Each slice would include electronic circuitry held in a supporting frame, which would contain the features needed for mechanical,

electrical, and thermal connections to support insertion, removal, expansion, testing, and integration. Optionally, one could use external or internal input/output interfaces. Also, optionally, one could incorporate thermal insulation between slices or between modules.

Slices would be mechanically connected to adjacent slices via guide pins and retainers that would mate in the manner of plugs and sockets. Once the guide pins were inserted in the retainers, setscrews would be tightened to push on slanted guide-pin surfaces to generate contact forces. In a module oriented as in the figure, the contact forces between slices would be horizontal. The thermal path for each slice could be vertical and directly into a heat sink if the slice were bolted down onto the heat sink via the boltholes on the flange of its supporting frame.

This work was done by Don Hunter of Caltech for **NASA's Jet Propulsion Laboratory**. *Further information is contained in a TSP [see page 1].*
NPO-20362

Two Approaches to Improvement of InGaAs/InAlAs/InP HEMTs

It should be possible to increase gains and cutoff frequencies.

NASA's Jet Propulsion Laboratory, Pasadena, California

Researchers are following two approaches in an effort to improve the low-noise performances of InP-based high-electron-mobility transistors (HEMTs) that could be used as front-end amplifiers in millimeter-wave receivers. These devices are designed to operate while cooled to temperatures ≤20 K, where they function with high gain, low leakage, and the lowest noise levels of any transistors operating in the millimeter-wavelength range. However, the low-noise performances of these devices are still slightly below those of nontransistor state-of-the-art devices.

The two approaches to improvement are best explained with the help of a cross-sectional view of a typical InGaAs/InAlAs/InP HEMT (see figure). The first approach involves increasing the indium content, x, of the $In_xGa_{1-x}As$ channel layer, which is grown by molecular-beam epitaxy. Increasing x results in enhanced electron-transport properties, which translate to higher cutoff frequency and higher gain. Unfortunately, increasing x also increases the strain in the $In_xGa_{1-x}As$ layer with respect to the InP substrate; as a result, the thickness of the $In_xGa_{1-x}As$ must not be allowed to grow beyond a maximum critical thickness that decreases with increasing x. The thickness of the channel layer is important because the thickness of the quasi two-dimensional gas in this layer determines the quantum electron states and the confinement and density of electrons in the channel. If the channel is too thin, then the performance of the device is degraded.

In this research, devices are fabricated with channels of $x = 0.60$, 0.65, and 0.80 and corresponding thicknesses. In the case of the $x = 0.80$ channel, the indium content is not uniformly 0.80; instead, it is graded to a maximum of 0.80 to minimize the strain and thereby make it possible to grow the thickest possible channel layer while benefitting from the transports with the highest feasible x.

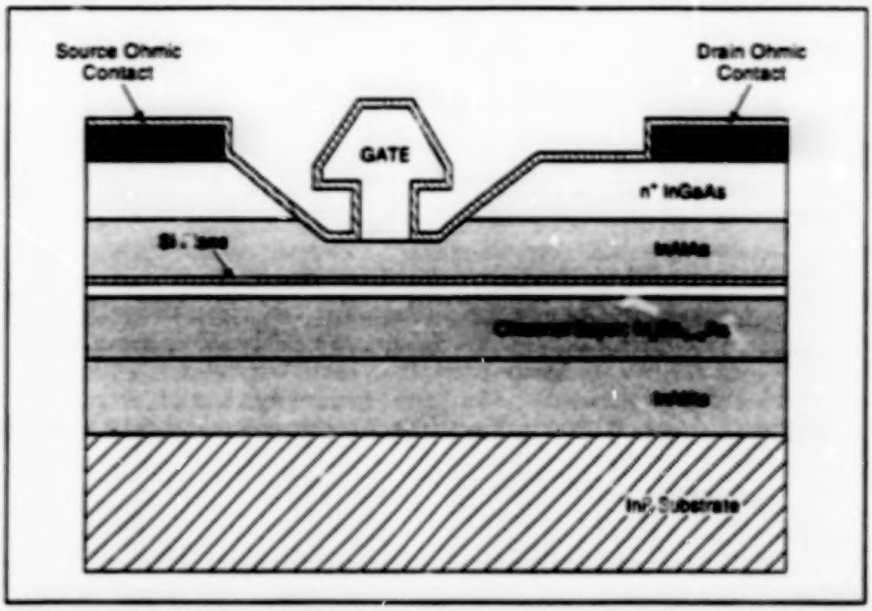

A Typical InGaAs/InAlAs/InP HEMT is depicted here in cross section (not to scale). Research directed toward improving low-noise performance has followed two approaches: (1) optimizing the indium content and thickness of the channel layer and (2) shortening the gate.

The second approach involves reduction of the gate length from 0.1 μm to ≤ 0.07 μm. Reduction of the gate length causes a reduction of internal capacitances, leading to lower noise, higher cutoff frequency, and higher gain. For example, decreasing the gate length to 0.07 μm can increase the cutoff frequency by as much as 25 percent.

There are two challenges to reduction of gate length. The first challenge is the difficulty of developing a high-yield manufacturing process to build 0.07-μm gates. Even electron-beam state-of-the-art electron lithography has thus far been limited to features with dimensions ≥ 0.1 μm. The second challenge is a short-channel effect: If the gate is too short, it cannot effectively pinch off the channel. This short-channel effect can severely limit device yield in mass production.

Both approaches have been followed in the fabrication of HEMTs in a dedicated 8-wafer lot split for the various indium compositions and gate lengths. The information gained from the devices on these wafers has provided insight on how to build the ultimate cryogenic millimeter-wave solid amplifier.

This work was done by Richard Lai of TRW Inc. for **NASA's Jet Propulsion Laboratory**. *Further information is contained in a TSP [see page 1].*
NPO-20341

DRAM Circuit Tolerates Single-Event Upsets

The equivalent of a majority vote is taken among triplicate memory cells.

NASA's Jet Propulsion Laboratory, Pasadena, California

A dynamic random-access memory (DRAM) circuit that tolerates single-event upsets (SEUs) has been developed. A single-event upset is a bit flip caused by ionizing radiation. In a DRAM, the state of each bit (0 or 1) is stored as charge on a buried capacitor. The impingement of an energetic charged particle can change the charge, and thus the state of the bit. There is no way to make a DRAM completely immune to SEUs, but the probability of a bit error in the DRAM output can be reduced significantly by use of redundancy; this is the concept on which the present SEU-tolerant design is based.

For protective redundancy, the DRAM incorporates three memory cells for each single cell that would otherwise be used. During recording, a bit is written in all three cells of a triple at the same time. Upon readout, the bit from the first cell is compared with that from the second cell; if the bits from the first and second cells are equal, then one of these bits is passed on to the data processor that requested the readout. If the bits from the first and second cells are not equal (because one was changed in an SEU), then the bit from the third cell is sent to the processor.

The comparison and selection of bits to pass on to the processor are accomplished by use of comparators and bus buffers. The SEU-tolerant DRAM also contains additional signal lines for full testing and for isolation and correction of faults.

This work was done by Steven Cole of Caltech for **NASA's Jet Propulsion Laboratory**. *Further information is contained in a TSP [see page 1].*
NPO-20474

Integrated Optical Voltage-Measuring Apparatus

This apparatus can measure high voltage safely and remotely.

John H. Glenn Research Center, Cleveland, Ohio

An integrated optical voltage-measuring apparatus based on a Mach-Zehnder interferometer has been designed and constructed. The main feature of this apparatus is that optical fibers link part of it to an optical sensor head placed at the source of the voltage to be measured, whether the source be a space-based power distribution control system or a ground-based high-voltage system. The optical fibers and sensor of this apparatus are immune to electromagnetic interference. This apparatus could be highly suitable for use in automatic control of space-based or aeronautical power-management and power-distribution systems. Potential ground-based commercial applications include measuring voltages and electric fields in electrical power systems, physiological monitoring and recording, measurements of pulsed power, and testing for electromagnetic compatibility.

Optical measurement of voltage involves utilization of the linear electro-optic effect, also known as the Pockels effect. Previously developed electro-optical voltage sensors have incorporated bulk electro-optic crystals and such bulk optical components as lenses, beam splitters, and polarizers. Because of the deficiencies in the design and construction of these devices, they have proved to be difficult to implement in the field. The use of bulk optical components can lead to difficulties in miniaturization, inadequate stability in outer-space applications, and high manufacturing costs.

The present integrated optical voltage-measuring apparatus overcomes these deficiencies of electro-optical voltage sensors made from bulk optical components. This apparatus is capable of measuring quasi-dc and ac signals at frequencies up to 3 MHz. It displays the true root-mean-square values of signals up to 200 V full scale. Its error is less than 2 percent of the full-scale reading. The maximum safe peak potential that can be applied to the optical head of this apparatus is 1,000 V. This apparatus also provides an analog output that can be used to display the measured waveform on an oscilloscope. The optical voltage-sensing head and the rest of this apparatus can be separated by a fiber-optic cable for remote measurement of high voltage.

The outstanding features, benefits, and capabilities of this apparatus, in addition to those described above, are the following:

- Optical isolation,
- Measurement of continuous-wave and pulsed signals,
- Large dynamic range,
- No need for electrical power at the sensor head,
- Possibility of placing the sensor head in a hostile or harsh environment, and
- Safe measurement.

This work was done by Stuart A. Kingsley and Sriram S. Sriram of SRICO, Inc., for **Glenn Research Center**.

Inquiries concerning rights for the commercial use of this invention should be addressed to NASA Glenn Research Center, Commercial Technology Office, Attn: Steve Fedor, Mail Stop 4–8, 21000 Brookpark Road, Cleveland, Ohio 44135. Refer to LEW-16731.

Forward-Link/Simulator PCI Card

Improvements include decreases in size, cost, and power consumption and an increase in speed.

Goddard Space Flight Center, Greenbelt, Maryland

The forward-link/simulator card (FLS) performs the fundamental satellite-telemetry data-transmission function for the forward (Earth-to-spacecraft) link in real time at rates up to 400 Mb/s. The FLS also simulates a Consultative Committee for Space Data Systems (CCSDS) telemetry data source that outputs data at rates up to 150 Mb/s, using industry-standard interface circuitry and standard connectors. Previously, at least two cards, each containing a central processing unit (CPU),

were needed to do what the FLS now does. CPU-based cards are complex; are expensive to build, operate, and maintain; are susceptible to malfunction; and require a great deal of power and cooling.

The FLS is a single industry-standard, full-length, 32-bit, 33-MHz, 5-V peripheral component interface (PCI) expansion card. In addition to the industry-standard PCI connector, it contains industry-standard subminiature B connectors for emitter-coupled-logic (ECL) input, an industry-standard DB-9 connector for RS-422 output, and a connector for programming nonvolatile logic devices. It contains an ECL output interface circuit, an RS-422 output interface circuit, a PCI bus interface application-specific integrated circuit (ASIC), three large reprogrammable nonvolatile logic devices, two large reprogrammable volatile logic devices, and miscellaneous active and passive devices.

In a typical data-source simulation, a test data pattern is loaded into a base pattern memory, control registers are set up by the host computer in which the FLS is installed and the card proceeds to generate test data automatically until it is stopped by the host computer. During typical forward-link operation, a pre-formatted uplink data stream, (comprising, for example, CCSDS telecommand frames), is loaded into a command buffer by the host, and the card proceeds to output the data automatically. Setup, control, insertion of data, and monitoring are performed through an entirely memory-mapped PCI interface by software running on the host computer.

In comparison with the previous assembly of at least two cards, the FLS is smaller, less expensive, faster, and more energy-efficient. The CPU-less, memory-mapped mode of operation of the FLS is simpler and more robust than was the CPU-based operation of the assembly of at least two CPU-based cards. The FLS is more flexible in that all logic is implemented in reprogrammable logic devices.

This work was done by Robert C. Kunz of RMS, Jason Dowling and Terry L. Graessle of Lockheed Martin, and Christos Kassiotos and David Fisher of SGT for **Goddard Space Flight Center**. *Further information is contained in a TSP [see page 1].*

GSC-14034

Special-Purpose Interface for Fast Writing on a Hard Disk

Size, weight, and power consumption are less than those of a general-purpose HDD interface.

Goddard Space Flight Center, Greenbelt, Maryland

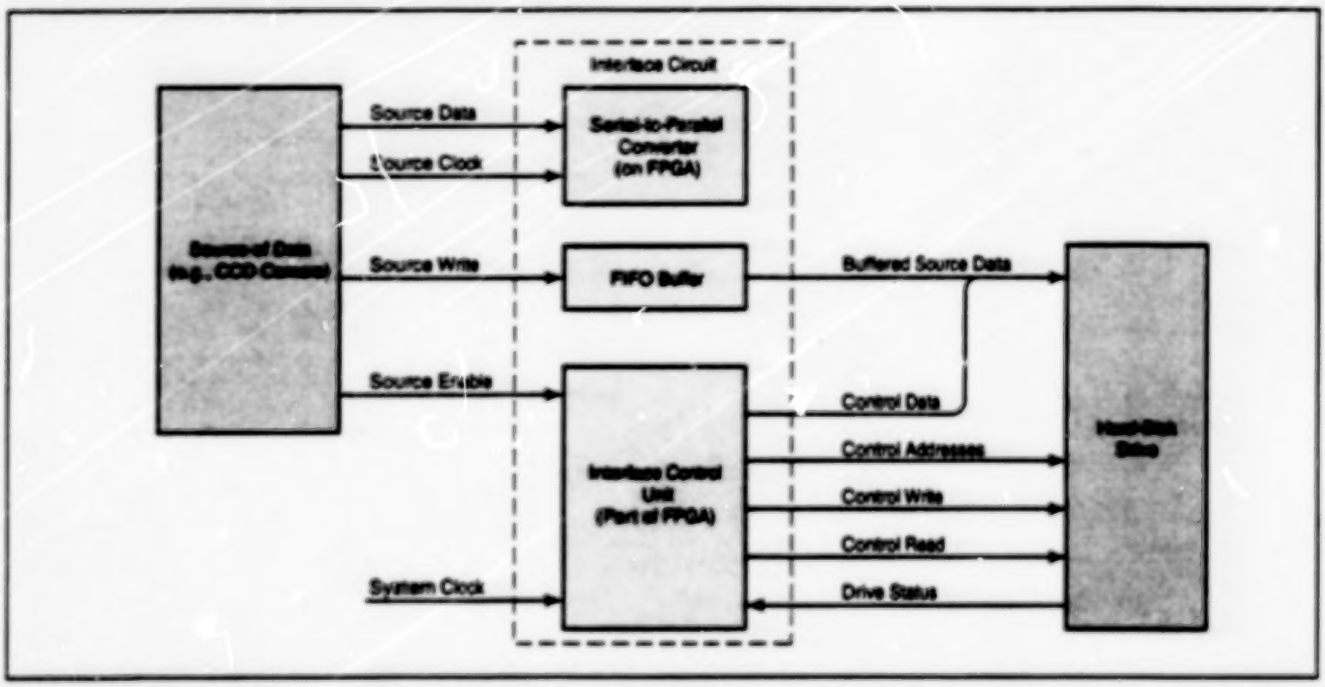

The Interface Circuit enables rapid writing of source data to sequential sectors on a hard disk. The interface circuit can be connected directly to any of a variety of commercially available HDDs.

A special-purpose interface circuit for a computer hard-disk drive (HDD) enables rapid writing of image data from a scientific instrument to sequential sectors on the hard disk. The design of this interface exploits the fact that most of the hardware and software components typically used to control the flow of data to the HDD of a general-purpose personal computer (PC) are not needed in a special-purpose instrument application; as a result, the size, weight, and power consumption of the data-storage portion of the instrument can be made less than they would be if a general-purpose interface were used. This interface can be connected directly to any of a variety of commercially available HDDs.

In the original application for which the interface was designed, the image data originate in a charge-coupled-device (CCD) camera that generates 12 bits per pixel, there being 3,072 pixels per line and 1,024 lines per image frame. Image data are read out from the CCD at a rate of 11.4Mb/s. Header information that is included with the data from each line increases the data rate to 15.2Mb/s. The HDD must be capable of accepting data at this rate to store complete images.

The interface (see figure) includes a serial-to-parallel converter, a first-in/first-out (FIFO) buffer, and a custom interface control unit. The serial-to-parallel converter and the

interface control unit are implemented on a field-programmable gate array (FPGA). The FPGA contains instructions in read-only memory (ROM) that initialize the HDD by use of an industry-standard interface protocol called "ATA-3." For each image line, the starting sector address is written to the HDD control registers. All of the source data (image data) pass through the serial-to-parallel converter, then through the FIFO buffer. The FIFO buffer can store several image lines simultaneously, making it possible for the control unit to wait while the HDD seeks the desired sector addresses.

After a complete line has been written, the control unit determines the status of the HDD and waits until the HDD is ready to receive more data. When the HDD is ready, it accepts header information, then accepts the source data. During acceptance of the source data, 16-bit words are written from the FIFO buffer to sequential HDD sectors at a system clock rate of 10 MHz. Later, stored data are retrieved from the hard disk by use of a separate commercial parallel input/output PC card.

Going beyond the original application, this interface can be used in other applications in which it is necessary to write data on sequential hard-disk sectors at high speeds. Because the interface includes an FPGA, it can be modified to satisfy requirements of different applications.

This work was done by Joseph Miko of **Goddard Space Flight Center**. *Further information is contained in a TSP [see page 1].*
GSC-14177

Electronic Systems

Hardware, Techniques, and Processes

15 Low-Power, Fast Machine Vision System on a Single IC Chip
16 Integrated Test and Operations System
17 SIBless Interface Design for Space-Station Training Computer
18 Apparatus Records Acceleration and Temperature
19 Radio-Frequency Wireless Flight-Control System
20 Retroreflective Communication Systems

BLANK PAGE

Low-Power, Fast Machine Vision System on a Single IC Chip

This system would function as an electronic "eye/brain machine."

NASA's Jet Propulsion Laboratory, Pasadena, California

A versatile, ultrafast, low-power machine vision system in the form of a single integrated-circuit chip has been proposed for use in military targeting, industrial robotics, and other applications in which there are requirements for utilizing visual information in real time. The conceptual design of the system takes advantage of recent advances in the design of integrated image-sensor/processor circuits, electronic neural networks, microprocessors, submicron very-large-scale integrated (VLSI) circuits, and massively parallel computation. The system could be characterized as an eye/brain machine (EBM) because the conceptual design is intended to mimic basic functions of biological vision systems. The system would be programmable to perform vision processing at all levels analogous to those of vision processing in the human eye and brain. The system would be capable of computation at the rate of 10^{12} operations per second — about 100 times the rate achievable with state-of-the-art microcomputers and digital signal-processing chips.

Figure 1 depicts the computational aspect of the conceptual EBM design. Visual information would be processed in five stages: (1) collection of raw images from sensors, (2) generation of synthetic images that augment raw images with additional information, (3) fusion of all images, (4) analysis of fused images, and (5) semantic interpretation of fused images.

The EBM would comprise the following two major subsystems:

- The EBM eye would be a compact optoelectronic subsystem that would integrate a variety of sensors with different geometric, radiometric, and spectral parameters chosen to satisfy requirements for a specific application.
- The EBM brain would be a high-performance control and data-handling subsystem that would contain most of the computational resources needed to perform machine-vision tasks.

An earlier version of the EBM, called the "Viewing Imager/Gimballed Instrumentation Laboratory and Analog Neural Three-Dimensional Processing Experiment" (VIGILANTE), was described in "Smart" Optoelectronic Sensor System for Recognizing Targets" (NPO-20357), *NASA Tech Briefs*, Vol. 22, No. 8 (August 1998), page 46. A prototype of the VIGILANTE was assembled largely from commercially available components. The conceptual design of the proposed system is based partly on lessons learned from the VIGILANTE prototype.

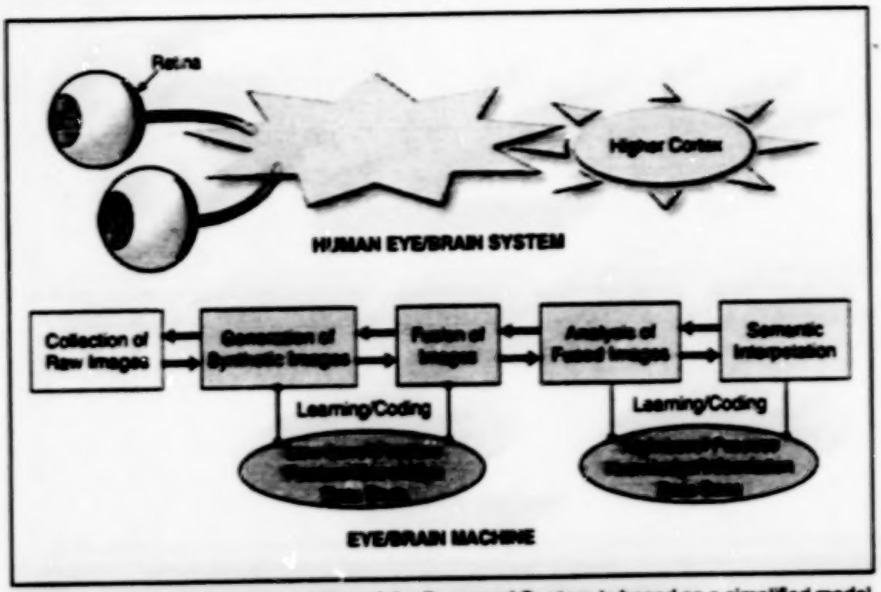

Figure 1. The Computational Aspect of the Proposed System is based on a simplified model of the human vision system, with five stages of processing of image data.

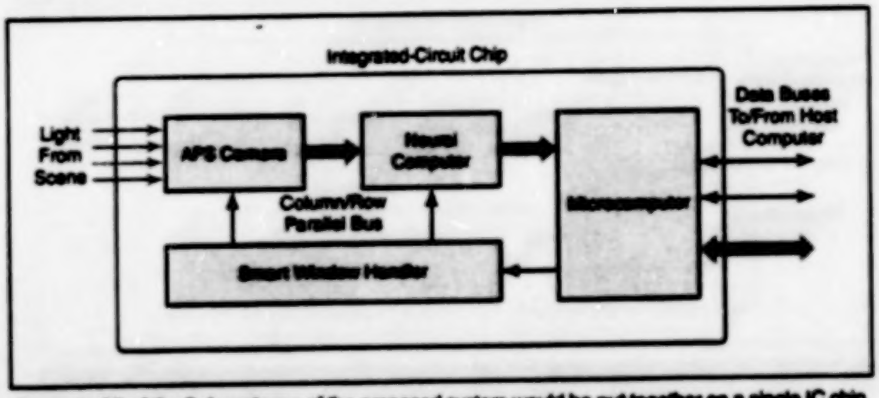

Figure 2. All of the Subsystems of the proposed system would be put together on a single IC chip.

Figure 2 depicts the electronic aspect of the conceptual EBM design. An active-pixel-sensor (APS) camera, a "smart" window handler, a programmable neural computer, and a microcomputer, and other subsystems would be put together on a single chip. All subsystems on the chip would be connected in a row/column-parallel image-data-flow architecture that would eliminate the data-bandwidth bottlenecks of older data-bus architectures.

The APS camera would constitute the array of sensors of the system. Under control by the "smart" window handler, windowed image data from the APS camera would be fed to the neural computer.

The neural computer would generate synthetic images, fuse all images, and analyze the fused images (stages 2, 3, and 4 of image-data processing) at a high speed that would be achieved by a combination of programmability and massively parallel computing structures. A prototype of the neural computer was described in "VLSI Neural Processors Based on Optimization Neural Networks" (NPO-19989), *NASA Tech Briefs*, Vol. 22, No. 1 (January 1998), page 58.

The microcomputer would control the overall operation of the system and would perform the scene-interpretation functions (stage 5 of image-data processing). The system could communicate with a host computer via a multibus interface unit.

The following are the anticipated advantages of building the system as a single IC chip instead of assembling it from components that are now commercially available:

- A higher degree of system-level integration could be achieved. System-level integration offers the capability to implement innovative parallel-processing architectures and ultrafast data-transfer structures while increasing the robustness of the system.
- The power consumed by the proposed single-chip system would be about 10 W, whereas a version of system capable of equal data throughput and assembled from commercially available components would consume about 100 W.
- Integration of all subsystems onto a single chip would entail shorter interconnections with fewer contacts and driver circuits, enabling the proposed system to operate at greater frame rates and processing speeds.
- The size of the proposed system would be about one-tenth that of the version of the system assembled from commercially available parts. The cost of mass-producing the system would be reduced accordingly.

This work was done by Wei-Chi Fang of Caltech for **NASA's Jet Propulsion Laboratory**. *Further information is contained in a TSP [see page 1].*
NPO-20449

Integrated Test and Operations System

This modular system is customized to specific applications through entries in a data base.

Goddard Space Flight Center, Greenbelt, Maryland

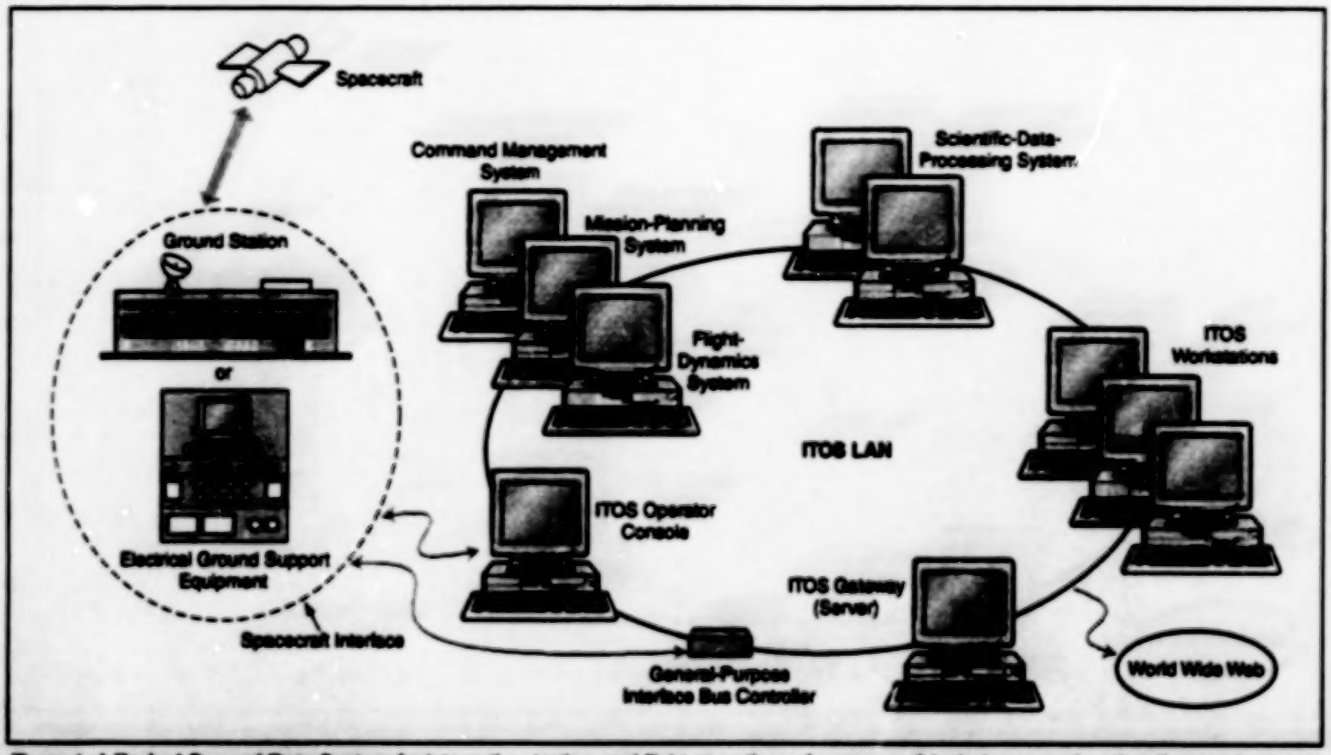

Figure 1. A Typical Ground Data System for integration, testing, and flight operations of a spacecraft includes several workstations and external systems connected via a local-area network.

The Integrated Test and Operations System (ITOS) is a generic system of software for controlling spacecraft and components of spacecraft during development, testing, and operation in orbit. The ITOS software is an inexpensive, portable, highly configurable system that runs under a variety of UNIX operating systems — including Solaris, FreeBSD, and Linux — on workstations or personal computers. The ITOS evolved from the ground support equipment built in 1990 to support integration and testing of SAMPEX, the first Small Explorer (SMEX) mission, and now is supporting SAMPEX and eleven other missions.

The ITOS software is executed on a cluster of workstations (see Figure 1) interconnected over a local-area network (LAN). Each workstation runs the complete ITOS software. One of the workstations is designated as the primary operator console; this console receives telemetry data from a spacecraft interface and sends commands to the interface via an Internet-Protocol (IP) Ethernet connection.

The primary console relays the spacecraft telemetry data to all other ITOS workstations on the LAN. Such computation-intensive operations as real-time, high-rate processing, distribution, and plotting of telemetric data can be distributed among workstations to achieve high performance at minimal cost of hardware. Each ITOS workstation unpacks the telemetry data packets and performs such data-processing tasks as limit checking, conversions of engineering units, and monitoring of configurations.

The primary ITOS console can distribute telemetry data, via an IP Ethernet connection, to external scientific, engineering, flight-dynamics, mission-planning, and command management systems attached to the LAN. These data are provided in a variety of formats and can be transferred by frame, packet, or individual datum. The ITOS uses a protocol that enables each of these external systems to request a particular type of data.

One ITOS computer can be connected to the Internet as a server to provide

telemetry and event displays that are viewable through any Java-capable web-browser software. This feature enables engineers to monitor and participate in tests and flight operations from remote locations, including their homes and offices. The server can also provide telemetry and event displays to the public via the Internet.

The ITOS software is customized from mission to mission, through an operational data base (which contains mission telemetry and command specifications), and through a small set of configuration files.

The ITOS can accept telemetry from multiple sources simultaneously. It can, for example, process spacecraft telemetry and ground-station status blocks or telemetry from a dynamic simulator. It can also control and monitor such external devices as receivers, bit synchronizers, and simulators by use of IEEE-488, RS-232, or network connections.

With respect to functionality, the ITOS software system can be characterized as divided into five subsystems: telemetry, command, control, data base, and events (see Figure 2). The telemetry subsystem contains programs for ingesting, unpacking, displaying, and checking telemetric data from spacecraft. The command subsystem contains programs for generating and transmitting spacecraft commands. The control subsystem includes programs for controlling and monitoring the spacecraft and the elements of the ground system. The data-base subsystem comprises programs for creating and gaining access to the operational data base. The event subsystem manages the recording, display, and forwarding of all messages generated by the ITOS programs and by the spacecraft.

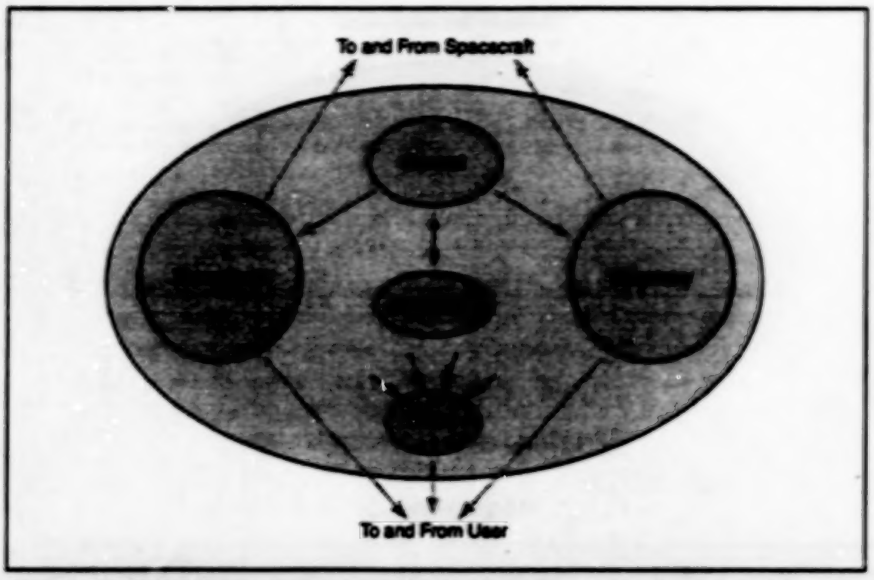

Figure 2. The ITOS Software System comprises five subsystems. The software is modular; most of its components can be replaced or augmented.

The cost of replicating the ITOS is low. This is partly because (1) the only commercial component of the ITOS software is a plotting program for which run-time licensing is not required and (2) the ITOS software is based on open standards. The ITOS software was developed by use of the Open Source GNU development suite. Its graphical user interface is based on Motif and the Java Development Kit. The development team made every effort to ensure that the ITOS code conforms to all relevant standards for maximum portability across UNIX implementations.

This work was done by Karen M. Keadle-Calvert and Sharon Osborne of Goddard Space Flight Center; Brian Goldman and Mark Richardson of AlliedSignal Technical Services; Danny Lewis of SGT; and Greg Greer, Tim Singletary, and Bruce Wendel of Hammers Company. Further information is contained in a TSP [see page 1].
GSC-14012

SIBless Interface Design for Space-Station Training Computer

Commercially available hardware and software are used.

Lyndon B. Johnson Space Center, Houston, Texas

NASA has developed a system of hardware and software that can accommodate all necessary interfaces between (1) space-station flight computers and (2) a simulation host computer used in training, with the least host-computer processing overhead, least cost, and least complexity. This system is said to be "SIBless" because it does not include a simulation interface buffer (SIB). The SIBless design is specific to the hardware and software systems of the station; it could also be moderately useful as a basis for similar systems in other applications that involve training simulation computers and data-acquisition systems that process large amounts of input and output (I/O) information.

The original design for space-station trainers called for a hardware and software system — a simulation interface buffer (SIB) — that would enable the host computer (a general-purpose avionics computer) to interact with all required devices. However, a redesign of the space station greatly affected this original requirement and led to the so-called SIBless design (see figure). The SIBless design succeeds on two levels: First, it succeeds as a means of quantifying the performances of various I/O methods. The analysis method involved in the SIBless design makes it possible to understand the architecture of the simulation host computer (an SGI Challenge XL computer) and to quantify the performance of this computer in different design alternatives. This analysis results in an understanding of the "sweet spots" and "dead spots" in the I/O performance of this computer with various commercial off-the-shelf interface cards and programs. Test results match estimates within about 5 percent.

The SIBless design also succeeds as one that requires few interrupts per frame. Analysis of the performance of the simulation host computer in handling VersaModule Eurocard (VME) and POWERchannel hardware interrupts revealed a need to reduce the number of interrupts as much as possible. A review of 1553-standard board vendors and an analysis of 1553 traffic characteristics and the SGI VME performance lead to a design that stayed within the "sweet spot" of the simulation host computer for some of the 1553 traffic; it also resulted in no interrupts for any of the 1553 traffic. The final design of a Small Computer Systems Interface (SCSI) device driver required only 1 interrupt per frame instead of the original 26 interrupts per frame.

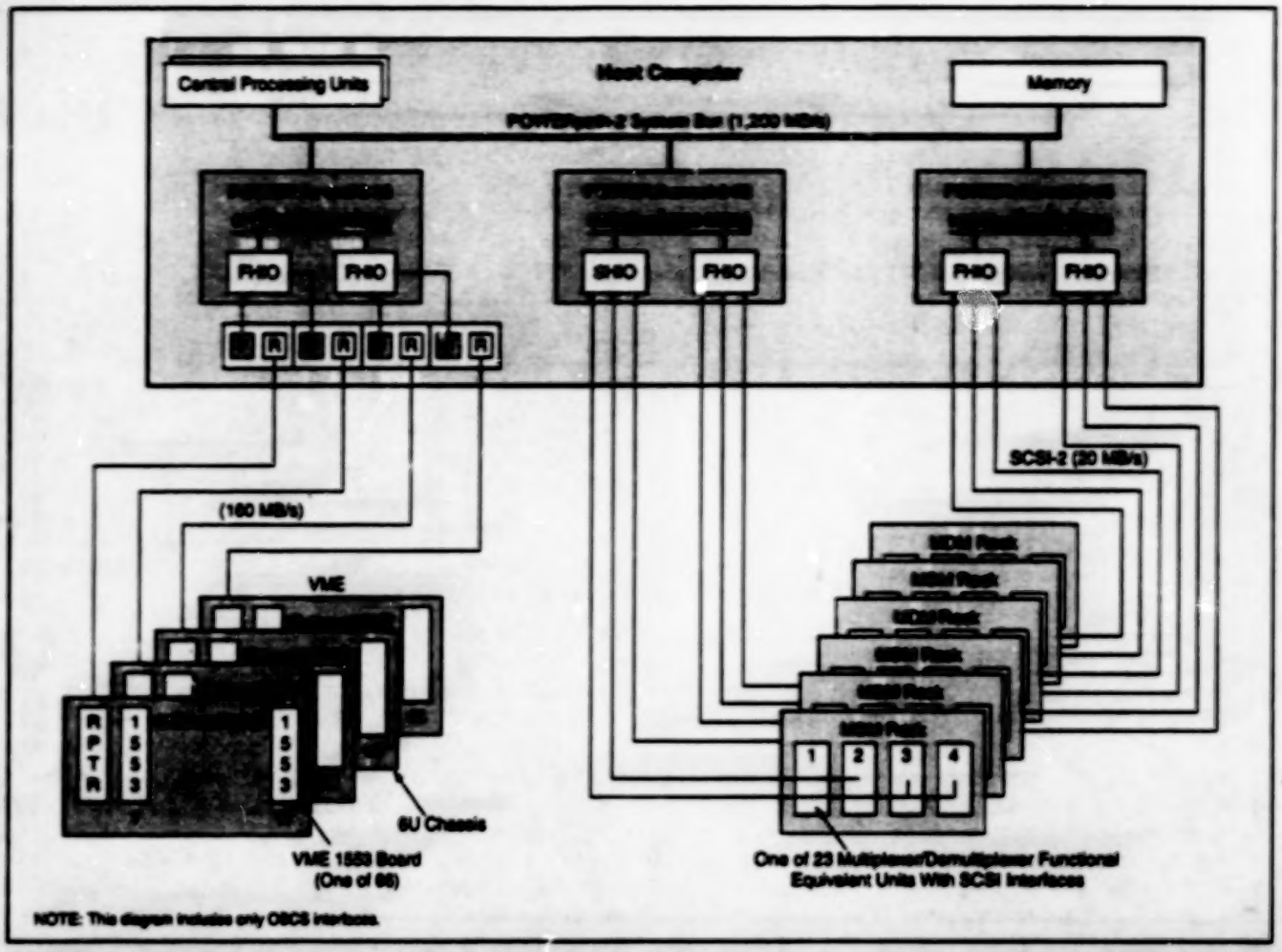

The SIBless Design accommodates all necessary interfaces in the original application, with the least host-computer processing overhead, least cost, and least complexity.

The novelty of the SIBless design is that it provides an example of how much I/O can be accomplished when a simulation host computer is used in real time and engineers employ a smart design. Although it is only a modified version of a previous design, the SIBless design succeeds on a couple of levels because it can contribute to significant cost and time savings. Unfortunately, its commercial applications are limited because it was designed for space-station support.

This work was done by Robert Horton and Cary Cheatham of Hughes Training and Dave Thornton of Loral for Johnson Space Center.
MSC-22765

Apparatus Records Acceleration and Temperature

An apparatus records triaxial acceleration and temperature as a function of time, operating unattended for as long as 3 weeks on power supplied by two D cells. The apparatus, which has dimensions of only 3.5 by 4.5 by 2.2 in. (8.9 by 11.4 by 5.6 cm) and weighs only 28.5 oz (0.81 kg) is designed primarily to be attached to an article of commerce to log the shock, vibration, and temperature to which the article is exposed during shipment. The apparatus contains three digital accelerometers. It is easily programmed through a serial link to a desktop or notebook computer running Windows 95. When activated, the apparatus stores up to 8 MB of acceleration and temperature data in nonvolatile memory. The acceleration data can be stored as sampled (or, for efficient utilization of memory, can be preprocessed into such parameters as peak or root-mean-square acceleration or velocity) at a rate from 1 to 4,000 samples per second. The stored data are subsequently downloaded to a personal computer for display and analysis.

This work was done by John C. Cole of Silicon Designs, Inc., for Kennedy Space Center.

In accordance with Public Law 96-517, the contractor has elected to retain title to this invention. Inquiries concerning rights for its commercial use should be addressed to

John C. Cole, President
Silicon Design, Inc.
1445 N.W. Mall Street
Issaquah, WA 98027
(425) 391-8329

Refer to KSC-11969, volume and number of this NASA Tech Briefs issue, and the page number.

Radio-Frequency Wireless Flight-Control System

Mechanical-cable, hydraulic, and wire control links would be replaced by RF links.

Dryden Flight Research Center, Edwards, California

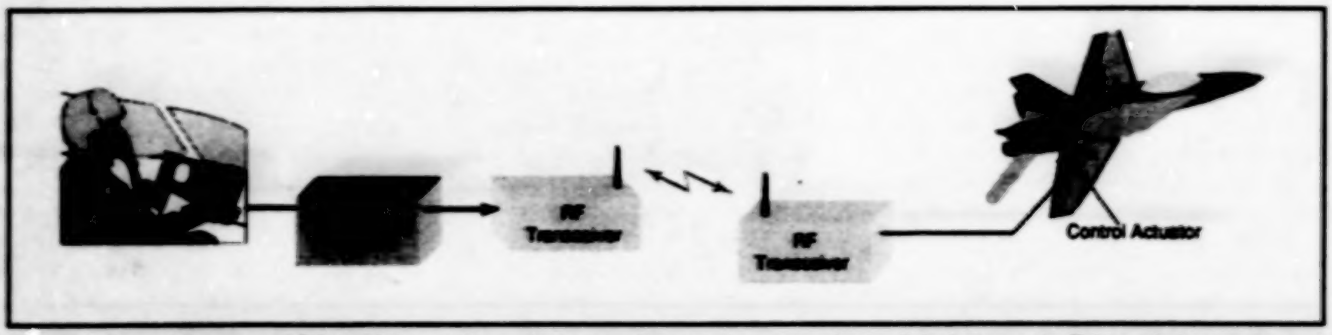

Figure 1. Spread-Spectrum RF Data Links would supplant or supplement wire communication links between the flight-control computer and the actuators for the flight-control surfaces.

Technological advances have driven the evolution of aircraft flight-control systems. In the dawn of 20th-century aviation, the Wright Brothers used cables and warping of wing surfaces to change the shapes of flight-control surfaces. As engineers designed aircraft capable of flying faster, higher, and farther, the forces needed for controlling the aircraft surpassed the physical abilities of pilots. Hydraulics were introduced to provide the pilot with the capability to manipulate the flight-control surfaces on the wings and tail of the aircraft. NASA Dryden Flight Research Center (DFRC) has been instrumental in effecting the continuing evolution of aviation technology by exploring ways of replacing hydraulics with "power by wire" actuators; an instance of this effort was reported in "Designing Electrically Powered Actuators for Aircraft" (DRC-98-09), *NASA Tech Briefs*, Vol. 21, No. 10 (October 1997), page 84.

On the verge of the next millennium, NASA DFRC is once again involved in the next major aviation milestone: a wireless flight-control system (WFCS), in which radio-frequency (RF) links would supplement or supplant wire flight-control connections. The ultimate goal is to develop a closed-loop WFCS that will be used to either (1) back up a wired system and provide redundancy for enhanced safety and reliability or (2) replace the wired system and decrease the size, weight, and cost of the affected aircraft.

The WFCS concept (see Figure 1) involves the insertion of spread-spectrum RF data links into the communication paths between the flight-control computers (FCCs) and the actuators for the flight-control surfaces at the ailerons, rudder, and elevators. For a demonstration of the feasibility of this concept, a prototype system (see Figure 2) was designed and demonstrated on the F-18 Iron Bird test facility at Dryden Flight Research Center to establish the ability of the RF links to provide adequate control capability. For demonstration purposes, the testing was limited to the signal paths between the FCCs and an aileron on the Iron Bird.

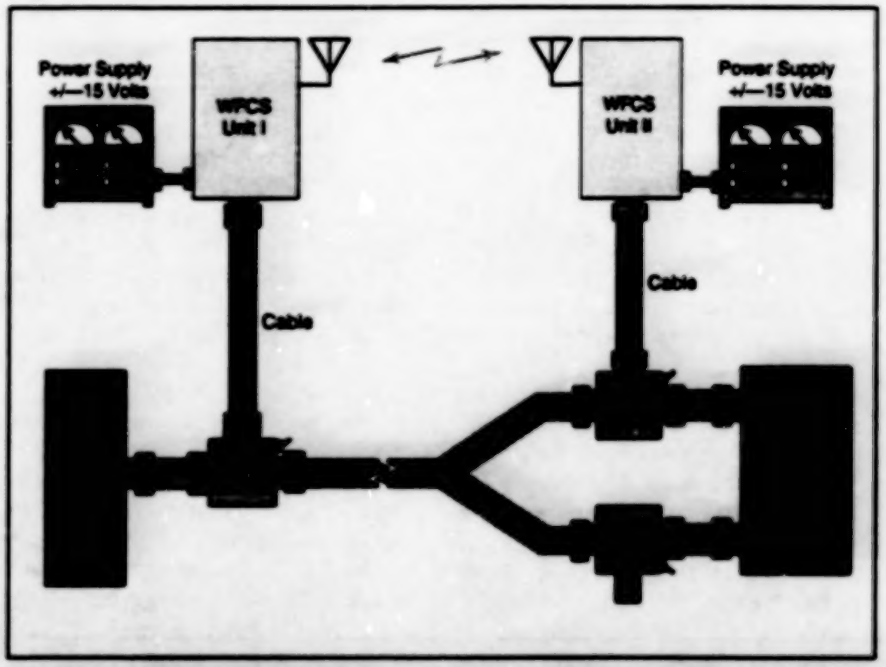

Figure 2. A Prototype WFCS System was tested to establish the capabilities of its RF links. The testing was limited to the signal paths between the FCCs and the actuator of one aileron.

The RF hardware in the test system includes an input module that receives and sends analog signals to and from the FCC and the control-surface actuators. These analog signals are converted to and from digital values by analog-to-digital and digital-to-analog circuits. The converted analog signals are passed to buffers that are set up in the memory spaces of WFCS computers. From these spaces, digital control movement data are encoded into messages that contain the movement information as well as synchronization and channel-identification data. These messages are then passed to the baseband processor of a spread-spectrum radio transceiver. Here, the baseband data are multiplied with randomized redundant data and sent to a modulation processor.

The modulation processor commands the RF section of the transceiver by phase-encoding the data "chips" to be transmitted. The RF section then transmits the data via a phase-modulated carrier signal. The receiver performs the inverse process that results in an analog signal that replicates the analog command input from the FCC.

For the proof-of-concept test, the data-link hardware was constructed in "breadboard" form. There was no attempt to

miniaturize the hardware at this stage of development. The idea was only to prove that the bandwidth of the spread spectrum was sufficient to satisfy a requirement for timing in an inner control loop. Power for the data link was provided by bench-top power supplies. Considerable effort was spent to make the power-supply lines between the bench supplies and the data-link hardware as short as possible so as to shield the power supply lines from outside electromagnetic interference. The data-link transceivers were placed at locations for which there was no line of sight between the transmitting and receiving antennas; thus, communications during the test took place entirely by multipath propagation. The antennas were simple monopole structures with no ground planes.

The WFCS hardware was completely software-driven, with the exception of the analog input and output needed to satisfy the analog front ends on the FCCs and the actuators. The software was designed carefully to maintain a minimum of phase and latency error while sampling the control signals at sufficiently high rates to insure accurate representations of the waveforms without filtering that would inherently introduce phase errors. Analog signals were captured from several locations in the system during the test to verify that the wireless system was reproducing the analog control signals with adequate fidelity. Manual commands were also used to test the full dynamic range of the wireless system and its ability to move the aileron to its maximum extent.

This system performed reliably after installation and debugging. Noise was reduced by shielding the power-supply wires against electromagnetic interference along their full lengths. Junction boxes that contained pass-through wiring were covered by foil tape; this provided shielding against electromagnetic interference (including RF interference) for the signal paths that remained hard-wired. Considerable experimentation was done to explore the size and distribution of the near-field diffraction and interference patterns associated with the hangar and the placement of the airframe in the line-of-sight path between the wireless transceivers.

The wireless system provided control of the aileron that was equal to the control provided by the production system supplied with the aircraft. The hardware was switchable into and out of operation at any time. One box controlled the signal paths through the aileron actuator. Another box controlled the signals from the FCC. When the control switches were placed in the "pass through mode" position, the Iron Bird flight-control system operated normally. When the control switches were placed in the "RF mode" position, the WFCS digital RF data link passed the control data for the actuator servo valve to control movement of the aileron.

The WFCS was tested for frequency, stability, and amplitude response, using the same test criteria ordinarily used to determine the fitness of the aircraft for flight. The RF system satisfied all the closed-loop-control timing requirements. The RF spread-spectrum system operated in under the non-line-of-sight condition throughout the test, with no direct path between the transceivers. In fact, the devices were positioned so that the entire bulk of the F-18 was in the center of the direct path between the two transceivers.

The demonstrated feasibility of the prototype system provides a solid base on which to proceed to the next stage of development. Future efforts will include more extensive testing in progressive phases and implementation of carrier suppression and code diversity multiple access (CDMA) techniques. The development effort is expected to culminate in a flight test that will include flight-dynamics demonstrations with and without the RF system in operation. The test is also expected to include operations in jamming environments designed to simulate worst-case accidental interference conditions.

This work was done by Sangman Lee, Linda Kelly, and Arthur Lavoie of **Dryden Flight Research Center** *and Karl Kiefer and Kevin Champaigne of Invocon Inc. Further information is contained in a TSP [see page 1].*

In accordance with Public Law 96-517, the contractor has elected to retain title to this invention. Inquiries concerning rights for its commercial use should be addressed to:

Karl Kiefer
Invocon Inc.
19221 IH-45 South Ste. 530
Conroe, TX 77385.

Refer to DRC-99-08, volume and number of this NASA Tech Briefs *issue, and the page number.*

Retroreflective Communication Systems

This system provides two-way communication with one transmitter.

Lyndon B. Johnson Space Center, Houston, Texas

A retroreflective communication system (RCS), is a state-of-the-art system that provides (1) two-way optical communication using only one transmitter and (2) multipath communication among remote locations. RCSs were conceived for use in communication among stations on the ground and aboard spacecraft in flight.

In the basic mode of operation of an RCS, a laser beam is transmitted from a first station to a second (remote) station that is equipped with a precise retroreflector and a light modulator. The second station can thus modulate the beam with new information and return the beam to the first station. The second station is characterized as passive in the limited sense that it does not contain a laser or other transmitter. Because of this passivity, the size, weight, and power consumption of the second station can be much less than in other communication systems; these characteristics make the RCS particularly attractive for spacecraft communications.

Other spacecraft communication systems can include repeaters mounted on towers or launched into orbit to extend their ranges and/or to enable transmission over the horizon. A typical repeater in such a system consists of a receiver and a transmitter connected to one or more antennas (in a radio system) or lens subsystems (in an optical system). Complicating matters, orbiting transmitters and receivers are often powered by batteries that must be recharged by solar photovoltaic arrays. For long-range communication, the amount of power that must be provided to a transmitter is several orders of magnitude greater than that needed to operate the associated receiver. Therefore, electrical subsystems must be sized to satisfy the peak power demands of transmitters. When multiple remote sites receive simultaneous communications from a transmitter, its power must be shared among these sites. Not surprisingly the weight, size, and complexity of a power system, a transmit-

ter, and an antenna launched on a satellite significantly affect the cost of launching. Yet another disadvantage of maintaining a transmitter in orbit is that the satellite that carries the transmitter must be repeatedly repositioned for precise pointing of the transmitted beam(s). Because of the large amounts of energy that must be expended to reposition the mass of the communication equipment and the rest of the satellite, the useful orbital life of the satellite is limited by the consumption of fuel.

By reducing the consumption of power in a communication satellite, the design of a low-bandwidth RCS can reduce the use of fuel and thereby the increase the useful orbital life of a satellite. The modulator in a passive RCS unit is a liquid-crystal shutter (LCS) that varies the polarization of a beam of light. An LCS, which functions similarly to the liquid-crystal display in a wristwatch, is powered by a photocell that generates power when exposed to light from a transmitting source. An LCS consumes so little power that a button-sized lithium cell could well support continuous operations for several years. Although, such practical limits as bandwidth and temperature extremes might alter this, an RCS should be capable of communicating data from the Moon to the Earth by use of a laser transmitter and an optical telescope, expending little more energy at the Moon site than is used to power an LCD wristwatch.

Another strength of the RCS is its ability to dramatically reduce requirements for precise aiming. In an RCS, any number of locations on Earth could simultaneously receive information from a passive unit on the Moon, using a few precise points. A typical envelope for capturing and returning a beam of light by a single retroreflector is a 22°-half-angle cone about the main optical axis of the retroreflector. One can group together multiple retroreflectors aimed at different angles to increase the effective capture-and-return envelope. The pointing requirements for communication at extreme distances are dictated only by the capture-and-return envelope. Because the divergence angle of a beam returned by a typical precise retroreflector is ≤1 arc second, a significant fraction of incident light is returned to its source.

An RCS could be used, for example, to communicate information from an active unit on Earth to a similar unit on the Moon, where such information would be stored and reflected back to a second active unit on Earth. In fact, retroreflectors left on the Moon during lunar landings in the 1970s have already been tracked from Earth with laser apparatuses similar to those of RCSs. RCS remote units could also reflect information from microrover landers to parent spacecraft orbiting a planet.

For spacecraft communications, the RCS concept offers the potential for major improvement over systems now in use. Reduced weight and size, the possibility of minimizing transmitting antennas and pointing requirements, and a passive design (consumption of little electrical power and generation of negligible heat) place the RCS concept ahead of its competitors. These characteristics could be exploited to reduce the fuel-to-weight ratios of support spacecraft, thereby promoting deeper penetration of outer space for exploration. Though utility is largely limited to outer-space applications like those described above, RCSs might be useful in some terrestrial applications because the RCS concept offers a unique combination of passiveness of a remote station, a secure link, and very low power or self-powered operation of the remote station; no other communication system offers this combination of features.

This work was done by Leo G. Monford, Jr., of **Johnson Space Center**. *Further information is contained in a TSP* *[see page 1]*.
MSC-22781

BLANK PAGE

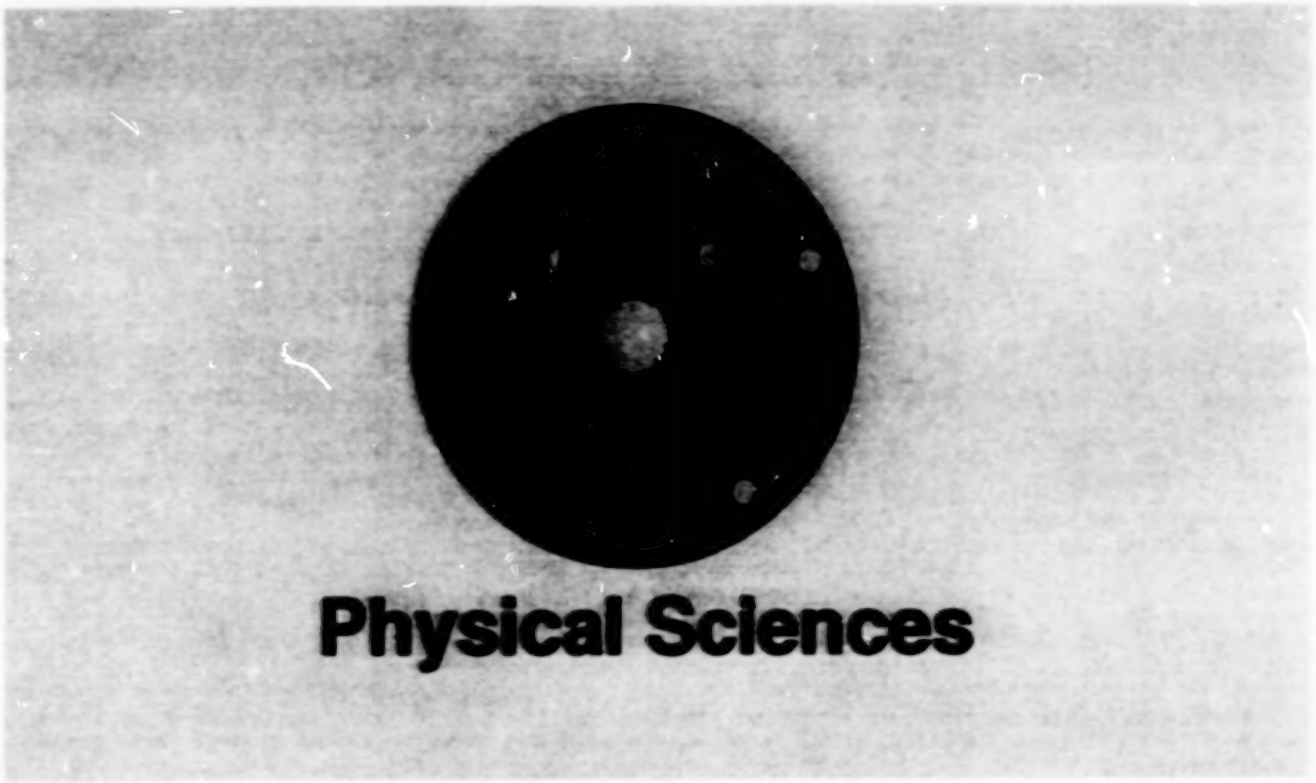

Physical Sciences

Hardware, Techniques, and Processes

25 AlGaN Photodiodes Respond to Ultraviolet C
26 Rayleigh-Scattering Measurement of Temperature and Velocity
28 SiC-Based Black-Body Absorbers for Submillimeter Wavelengths
29 Mass-Produced Hollow Cathodes Will Cost Less
30 Software for Precise Ultrasonic Contact Measurements
31 Parallel 3D EMPIC Algorithm Using Nonorthogonal Grids

BLANK PAGE

AlGaN Photodiodes Respond to Ultraviolet C

These are solar-blind photodiodes, for which there are numerous potential uses.

Dryden Flight Research Center, Edwards, California

Solar-blind photodetectors respond only to ultraviolet light at wavelengths shorter than those of the solar radiation that can penetrate atmosphere of the Earth. This wavelength range, traditionally defined as wavelengths <280 nm, is known as ultraviolet C (UV-C). Terrestrial solar light in this range is absorbed in the atmosphere, primarily by ozone, and does not reach the ground. However, UV-C radiation can also be produced on the ground by such combustion processes as forest fires, artillery fire, or missile launches. Detection of UV-C under the atmosphere without background interference from longer-wavelength solar radiation can serve to identify these terrestrial fire sources. Solar-blind detectors include gas-ionization chambers (e.g., Geiger-Muller tubes) and conventional photodiodes and photomultipliers when used in combination with blocking filters and phosphor down-conversion techniques.

The material system that consists of nitrides of elements of column III of the periodic table offers the potential for solid-state photonic devices that are inherently solar-blind. These materials are a subset of the semiconducting compounds that comprise elements from columns II and V of the periodic table. More familiar III-V semiconductors include GaAs, GaP, and such ternary variations as AlGaAs. The distinctive aspect of the III-nitrides is that their bandgaps fall in the energy range that corresponds to blue and ultraviolet wavelengths. The bandgap of a ternary III-nitride material, (e.g., InGaN or AlGaN) can be tailored by varying the proportions of the column-III elements. For example, the bandgap of $Al_{0.37}Ga_{0.63}N$ is 4.4 eV, which, as a photon energy, corresponds to a wavelength of 280 nm — the long wavelength edge of the UV-C band. In comparison, silicon, the most common semiconductor material for photodetectors, has a bandgap of 1.1 eV, corresponding to a wavelength of 1.1 μm, which is in the infrared region.

AlGaN Schottky photodiodes that respond primarily to radiation in the UV-C spectral band have been developed. Single-element Schottky photodiodes, each having an active area of 0.5 mm^2, have been fabricated. The AlGaN layers of such a device are deposited by molecular beam epitaxy (MBE) on a sapphire substrate. The device consists of an underlying 0.5-μm-thick n^+ layer of AlGaN doped with silicon and an overlying 1.0-μm-thick layer of undoped AlGaN. Standard photolithographic techniques are used for patterning the device. Inductively coupled plasma (ICP) etching is used to form a mesa of undoped AlGaN layer and expose the underlying n^+ layer for ohmic-contact metallization. A semitransparent nickel layer is used for the Schottky contact on the undoped AlGaN layer.

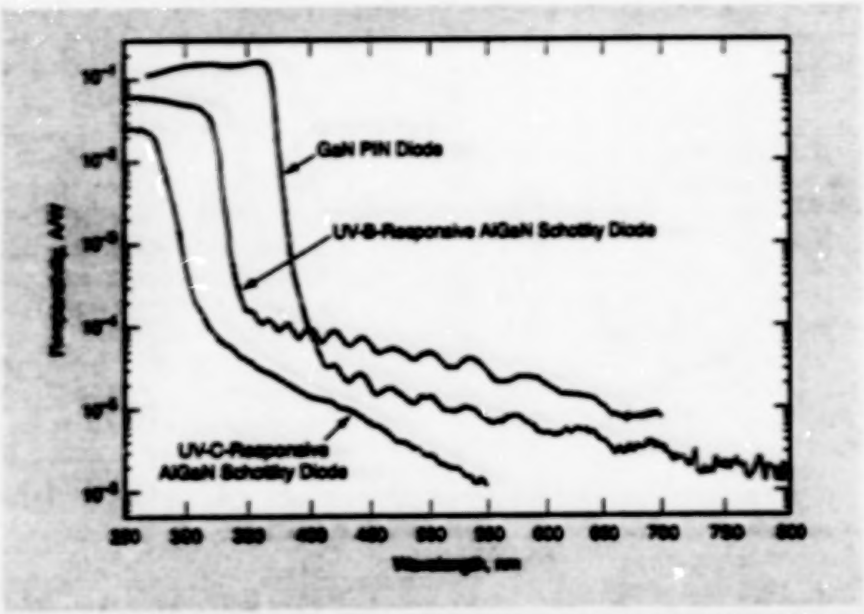

Figure 1. The Photovoltaic Spectral Responsivities of three column-III nitride photodiodes are plotted together for comparison.

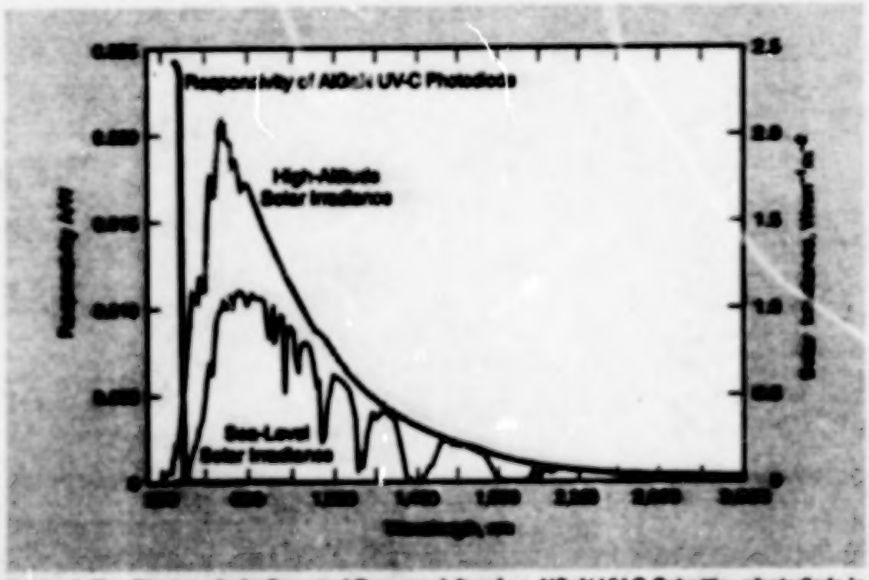

Figure 2. The Photovoltaic Spectral Responsivity of an AlGaN UV-C Schottky photodiode is overlaid on solar irradiance spectra from above the atmosphere and from sea level to show that the AlGaN UV-C photodiode is blind to solar light that penetrates the atmosphere.

Figure 1 depicts the photovoltaic spectral responsivity of a UV-C-responsive photodiode of this type. Also shown for comparison is the responsivity of an $Al_{0.17}Ga_{0.83}N$ Schottky photodiode that exhibits a peak response at 320 nm (the long-wavelength cutoff of UV-B) and the responsivity of a GaN p-type/intrinsic/n-type (PIN) photodiode that exhibits a peak response at 365 nm.

The logarithmic responsivity scale of Figure 1 helps to emphasize the long-wave-

length rejection of the UV-C-responsive photodiode. The response of this photodiode at a wavelength of 370 nm is only 10^{-3} times its peak response. As the wavelength increases to 500 nm, the response falls another order of magnitude, and as the wavelength increases further to 650 nm, the response decreases to 10^{-5} times the peak response. With its peak response at 280 nm, the UV-C AlGaN Schottky photodiode is the shortest-wavelength group-III nitride photovoltaic device demonstrated to date. The absolute response at 280 nm is considered to be fair. At 0.022 A/W it exhibits an external quantum efficiency of about 10 percent; this level of quantum efficiency is comparable to the quantum efficiencies of photocathodes in this spectral range.

Figure 2 shows an overlay of the responsivity of the UV-C sensor to the solar irradiance spectra at sea level and at high altitude. The AlGaN UV-C photodiode is blind to solar light at sea level because the portion of the sunlight in its spectral-response range is absorbed in the atmosphere.

Photodetectors made from column-III nitride compounds are uniquely well suited for numerous ultraviolet-detection applications, including sensing of flames in industrial settings, monitoring UV curing and drying, detection of arcs, controlling UV sterilization, monitoring UV in phototherapy, and solar-blind detection of fires. Because the column-III nitride material system is stable at high temperatures and during exposure to intense radiation, it is a good choice for photodetectors that must operate in harsh environments.

This work was done under a under 1998 NASA Phase I Small Business Innovation Research (SBIR) Contract by Jody J. Klassen, James VanHove, Robert Hickman II, Andrew Wowchak, Christine Polley, David King, Matt Rosamond, and Peter P. Chow of SVT Associates/Blue Lotus Micro Devices, Inc., for **Dryden Flight Research Center.**

In accordance with Public Law 96-517, the contractor has elected to retain title to this invention. Inquiries concerning rights for its commercial use should be addressed to

Jody Klassen
SVT Associates, Inc.
7620 Executive Drive
Eden Prairie, MN 55344-3677
Tel. No. (612) 934-2100 Ext. 247
E-mail: www.svta.com

Refer to DRC-99-25, volume and number of this NASA Tech Briefs *issue, and the page number.*

Rayleigh-Scattering Measurement of Temperature and Velocity

Further development of the temperature-measurement capability is needed.

John H. Glenn Research Center, Cleveland, Ohio

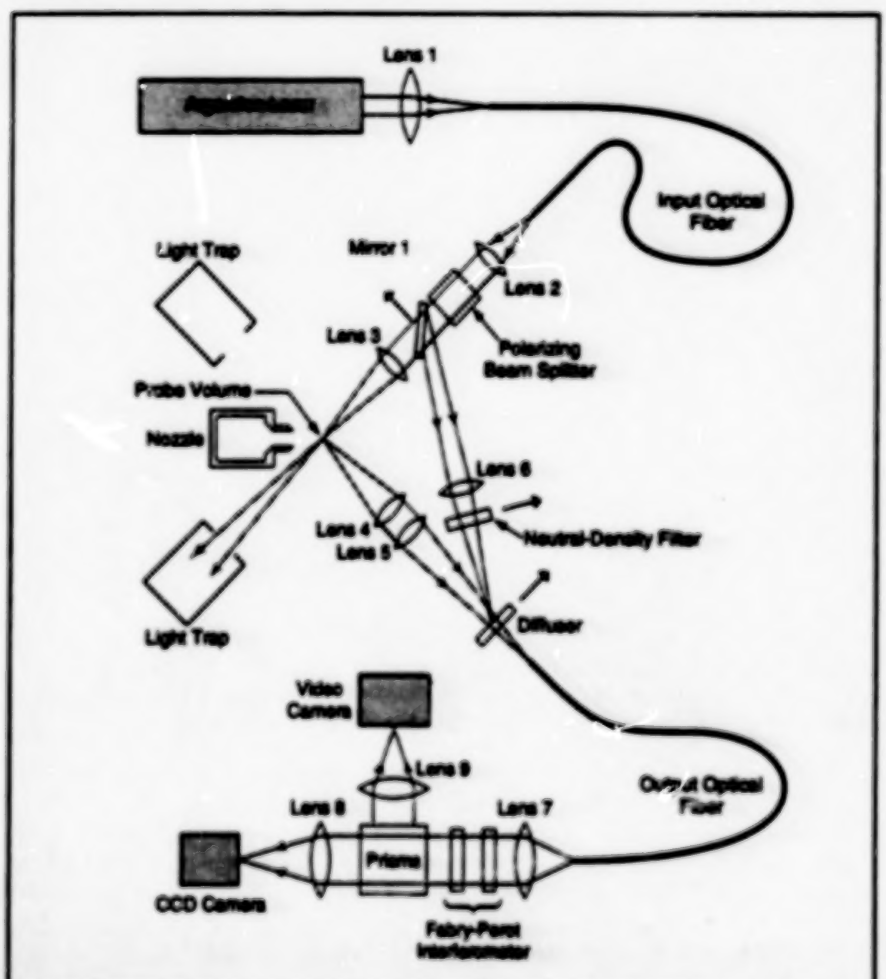

Figure 1. Rayleigh Scattering in the probe volume is excited and measured by remotely located equipment connected to the flow-test location by optical fibers.

Figure 1 schematically depicts an experimental setup in which Rayleigh scattering from molecules of a flowing gas is used to measure the temperature and one component of the velocity of the gas. The Rayleigh-scattering apparatus in this setup is capable of operation in the harsh environments (varying temperatures and intense vibrations and sound) commonly found in aerospace test facilities.

The power of Rayleigh-scattered light is proportional to the gas density, the spectral width of the scattered light is related to the gas temperature, and the shift in the frequency of the spectral peak is proportional to one component of the bulk velocity. Because the molecules of the flowing gas of interest are Rayleigh scatterers, no seeding of the flow is necessary. The concept of using molecular Rayleigh scattering to measure temperature and velocity has been reported previously. The novel aspect of the present Rayleigh-scattering apparatus lies in (1) the manner in which its delicate optical and electronic equipment are protected from the harsh flow-test environment and (2) the manner in which the Rayleigh-scattering spectrum is acquired and analyzed.

At the protected location, light from an argon-ion laser is focused by lens 1 into an input optical fiber, which delivers the light to the test location. There, the light is collimated by lens 2, then directed through a polarizing beam splitter. The light reflected by the beam splitter is directed into a light

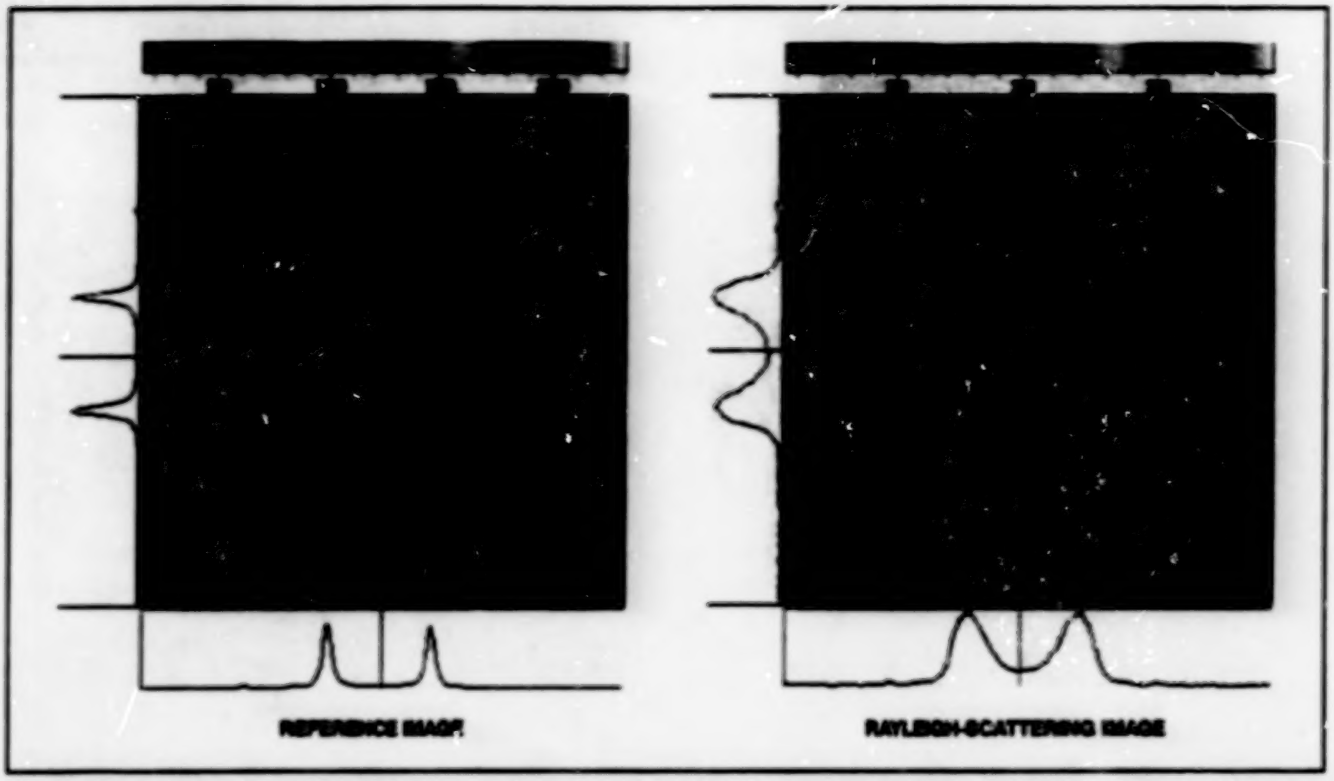

Figure 2. These Reference and Rayleigh-Scattering Images were generated in 10-second exposures. The Rayleigh-scattering image was acquired at a temperature of 297 K. In each case, a single fringe is shown, with horizontal and vertical plots of readouts from a single row and a single column of pixels through the center of the fringe.

trap (not shown in the figure); this light must be trapped because even though it would not contribute to the Rayleigh-scattering signal, it would contribute to detected stray light if it became depolarized when scattered from surfaces near the probe volume (the small volume from which Rayleigh scattering is to be measured). The beam transmitted by the beam splitter is focused into the probe volume by lens 3. Rayleigh-scattered light is collected by lens 4 and focused by lens 5 into an output optical fiber, which delivers the light back to the protected location.

The light coming out of the output optical fiber at the protected location is collimated by lens 7, then passed through a planar mirror Fabry-Perot interferometer operated in the static, imaging mode, then focused by lens 8 into a charge-coupled-device (CCD) camera cooled by liquid nitrogen.

Additional optics are included to provide for a reference Fabry-Perot image of non-Rayleigh-scattered laser light. These optics include a mirror that intercepts laser light coming out of the polarizing beam splitter. The light reflected by the mirror is focused by lens 6 through a neutral-density filter (if needed to reduce the intensity of the reference light) and a diffuser located in front of the output optical fiber. The diffusely scattered laser light then enters the fiber. The mirror, diffuser, and neutral-density filter are mounted on remotely controlled pneumatic linear actuators so that they can be moved into position for acquiring the reference image or moved out of the way for Rayleigh-scattering measurements. A prism assembly can be placed in the path between the Fabry-Perot interferometer and the CCD camera to direct light into a standard video camera.

The Fabry-Perot interferometer is aligned automatically on the reference image, then locked in alignment for acquisition of Rayleigh-scattering Fabry-Perot images. A five-parameter mathematical model of the instrument function is fitted to the digitized reference image. Thereafter, each Rayleigh-scattering Fabry-Perot image is digitized, then processed by an algorithm that, using the instrument-function parameters, finds the best fit of the image to a five-parameter mathematical model of the Rayleigh-scattering Fabry-Perot image; the fitting parameters are the amplitude of Rayleigh scattering, velocity, temperature, amplitude of stray laser light, and uniform background (see Figure 2).

In a test on a subsonic free air jet, velocities determined by Rayleigh scattering were in good agreement (within 5 m/s) with velocities calculated from isentropic-flow relations, but temperatures determined by Rayleigh scattering were not in equally good agreement. In a test on slowly flowing heated air, the velocities determined by Rayleigh scattering again agreed within 5 m/s, but the temperatures determined by Rayleigh scattering exhibited systematic errors on the order of 10 to 15 percent. Thus, it appears that the apparatus is capable of accurate velocity measurements, but that additional development of the temperature-measurement capability is needed.

This work was done by Richard G. Seasholtz and Lawrence C. Greer III of Glenn Research Center. Further information is contained in a TSP (see page 1).

Inquiries concerning rights for the commercial use of this invention should be addressed to NASA Glenn Research Center, Commercial Technology Office, Attn: Steve Fedor, Mail Stop 4–8, 21000 Brookpark Road, Cleveland, Ohio 44135. Refer to LEW-16747.

SiC-Based Black-Body Absorbers for Submillimeter Wavelengths

These absorbers can be fabricated at relatively low cost.

NASA's Jet Propulsion Laboratory, Pasadena, California

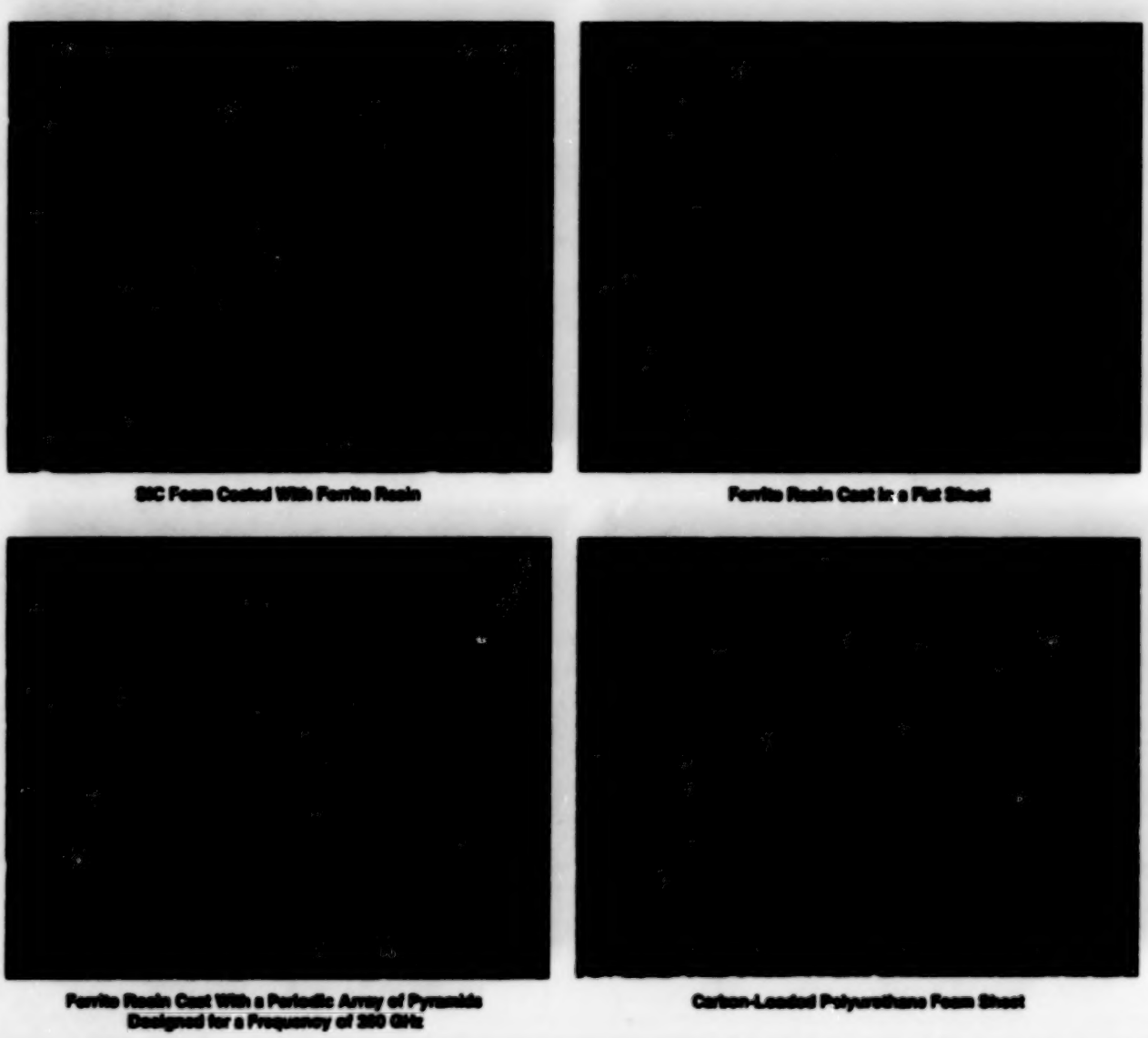
SiC Foam Coated With Ferrite Resin
Ferrite Resin Cast in a Flat Sheet
Ferrite Resin Cast With a Periodic Array of Pyramids Designed for a Frequency of 200 GHz
Carbon-Loaded Polyurethane Foam Sheet

Figure 1. A Panel of SiC Foam Coated With Ferrite Resin is shown at the same magnification with three panels of older competing designs. Tests at frequencies from about 120 to 640 GHz showed that the SiC-foam/ferrite-resin panel performed comparably to the panel with the array of pyramids, which cost much more.

Open-cell silicon carbide foam coated with a ferrite-filled absorbing resin has been found to be useful for black-body absorbers at millimeter and submillimeter wavelengths. The panels can be used as calibration targets for radiometers that operate at these wavelengths.

Heretofore, black-body calibration targets have been made from lightweight carbon-coated polyurethane foams or from heavy ferrite materials with machined or molded, finely pointed, periodic surface features (e.g., arrays of cones or pyramids) (see Figure 1). These black-body loads have either excessive weight, deteriorate (crumble) over time in vacuum, or have poor thermal conductivity.

The new loads are SiC-based, can be fabricated easily, are lighter in weight than solid ferrite absorbers, do not outgas excessively, and exhibit sufficient thermal conductivity for the intended purposes. Moreover, the silicon carbide base material withstands high operating temperatures.

The absorber works by effecting random scattering and surface impedance matching with absorption of power to produce a low return loss to incident radiation over a broad range of wavelengths. The open-cell foam structure is responsible for the scattering and impedance-matching properties. The ferrite coating increases the absorption coefficient without significantly changing

the scattering and impedance-matching properties.

The combination of roughness needed for random scattering and the impedance match to the radio-frequency field is optimized by choice of the foam cell size, which should be of the order of half the wavelength at the frequency of interest. SiC foam can be fabricated with foam cell sizes ranging from a few millimeters down to less than a tenth of a millimeter, corresponding to a frequency range from below 100 GHz to 1 THz or more.

The absorber is fabricated by pouring the castable ferrite resin over the open-cell SiC foam sheet and baking the sheet to cure the epoxy resin. Slabs can then be assembled in wedge or pyramidal geometries to enhance absorption (see Figure 2).

This work was done by Peter Siegel of Caltech and Robert Tuffias of Ultranet Corp. for **NASA's Jet Propulsion Laboratory.** *Further information is contained in a TSP [see page 1].*
NPO-20401

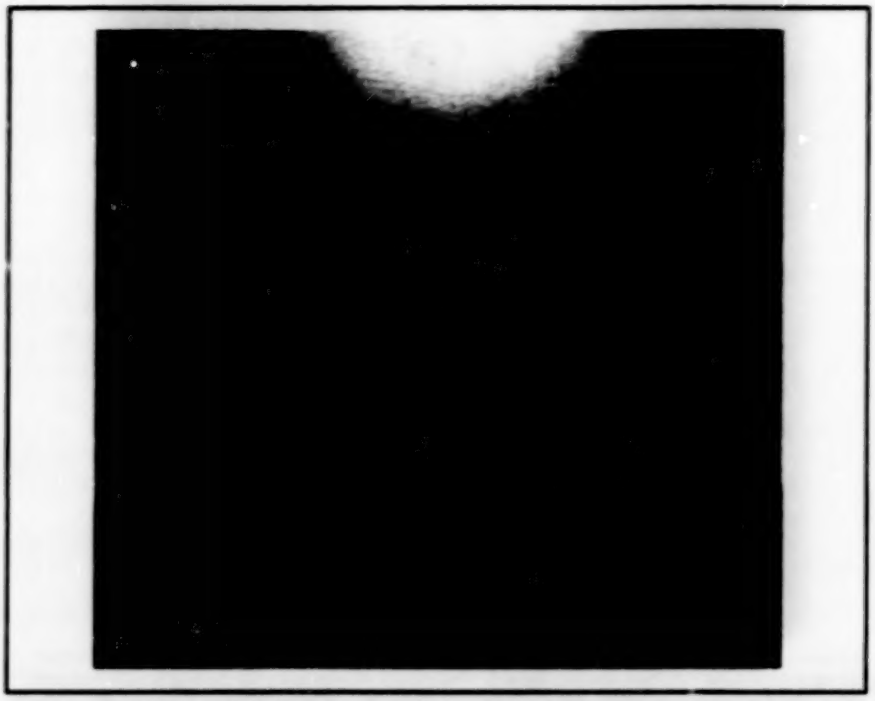

Figure 2. Two Coated SiC Panels are mounted in a wedge configuration to make incident radio-frequency energy undergo multiple reflections to enhance absorption. The panels measure 9 × 9 and 9 × 12 in. (229 × 229 and 229 × 305 mm), respectively. The wedge can accommodate a fairly wide beam but the thickness of the panels [0.5 in. (13 mm)] places the lower limit of operating frequency at about 100 GHz. The slots on the sides enable the adjustment of the dihedral angle between about 20° and 45° to obtain the best performance for a given beam diameter.

Mass-Produced Hollow Cathodes Will Cost Less

Design changes preserve functionality while enhancing manufacturability.

John H. Glenn Research Center, Cleveland, Ohio

A commercial version of the NASA plasma-contactor hollow-cathode assembly (PC HCA) has been developed. The NASA PC HCA is a highly reliable hollow discharge cathode that is the most thoroughly understood, tested, and mature of all hollow cathodes that have been considered for use in electric spacecraft thrusters. The design of the commercial version preserves all the critical aspects of the technological heritage of the NASA PC HCA necessary for long-term, reliable operation, while incorporating changes that enable mass production at lower cost per unit. Beyond the original intended spacecraft application, the commercial hollow cathodes could prove useful on Earth in plasma research and plasma-based manufacturing processes.

Like the NASA PC HCA, the commercial HCA (see figure) is a plasma source that utilizes an Xe or an Xe/Kr mixture as the feed gas and operates in conjunction with several power supplies, which are typically included within a power processing unit. Both the original NASA design and the commercial version call for a barium-

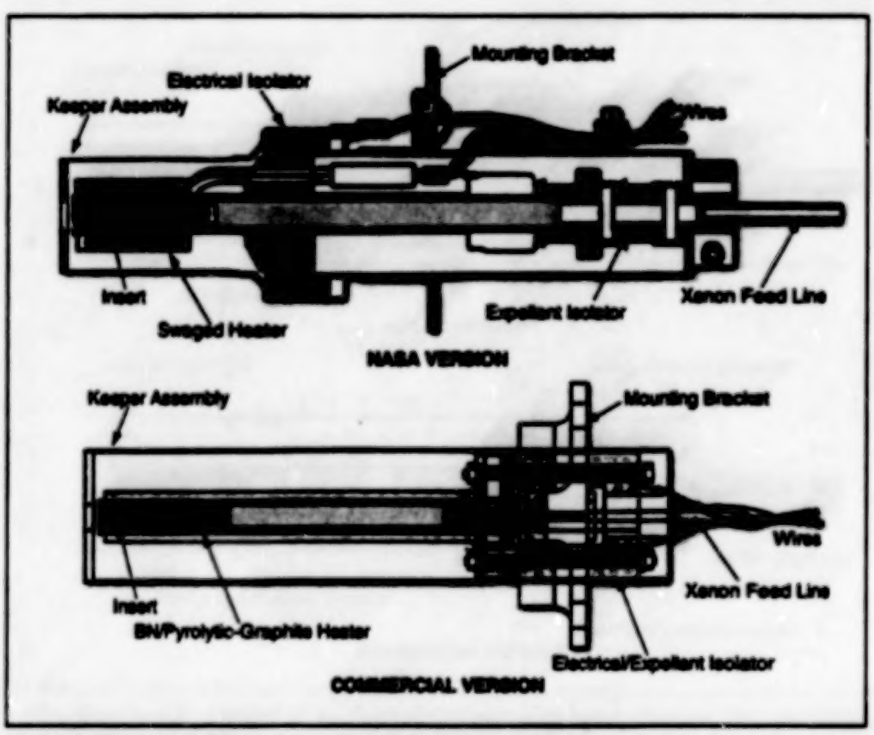

The Commercial Version of the Hollow-Cathode Assembly preserves the technological heritage of the NASA version, but can be mass-produced at lower cost.

impregnated tungsten insert housed within a 0.25-in. (6.35-mm) molybdenum/rhenium tube, and a molybdenum/tantalum keeper assembly, and both designs share an identical geometry and construction throughout a front subassembly wherein all the critical functions of the HCA take place.

There are only two major differences between the NASA and commercial versions. The first is the substitution of an advanced, commercially available heater for a laboratory-type helical swaged heater used in the NASA version. The commercial heater is expected to resist vibration better than the swaged heater does. The heating element in the commercial heater consists of pyrolytic graphite deposited on chemical-vapor-deposited boron nitride ceramic. Heaters of this type are very lightweight and can be operated at extremely high power densities.

A unique characteristic of heaters of this type is that their electrical resistances decrease with temperature up to about 1,000 °C; this characteristic makes it practical to use constant-voltage (instead of constant-current) heater power supplies. Another characteristic of the heater design include low unit-to-unit variability and precise tailorability of resistance. The net benefit afforded by these characteristics is to make it possible to reduce the complexity (and thus the cost) of power-supply circuitry and to increase the reliability of the heater, relative to those of the NASA PC HCA.

The second major difference between the two designs lies in details of the internal construction and mounting configurations in a rear subassembly. Modifications have been made here to enable cost-effective mass production.

This work was done by David Manzella of RMS Aerospace Engineering for **Glenn Research Center.**

Inquiries concerning rights for the commercial use of this invention should be addressed to NASA Glenn Research Center, Commercial Technology Office, Attn: Steve Fedor, Mail Stop 4–8, 21000 Brookpark Road, Cleveland, Ohio 44135. Refer to LEW-16658.

Software for Precise Ultrasonic Contact Measurements

This software performs control, analysis, and display functions.

John H. Glenn Research Center, Cleveland, Ohio

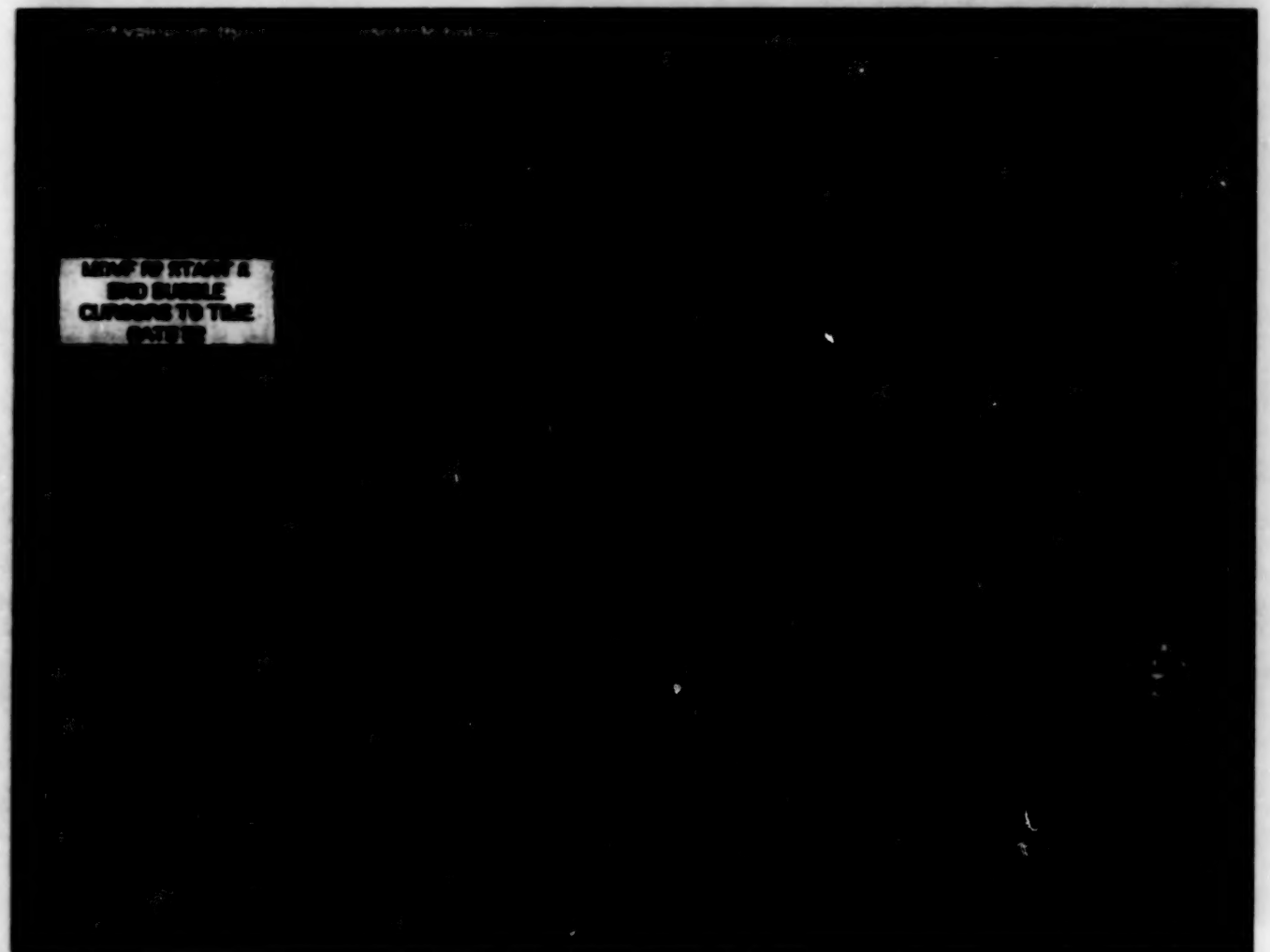

One of the ULTRA SON Displays is a window containing a raw time-domain waveform (ultrasonic-transducer voltage vs. time). This display prompts the user to enter the times when the front- and back-surface echoes are considered to begin and end ("B2" denotes the second back-surface echo), the voltage sensitivity level for the display, and the voltage offset control to enable calculation of frequency-based properties. The user can also specify the type of time-domain signal-processing window.

The ULTRA SON computer program is designed for use in precise ultrasonic contact scan measurements for nondestructive characterization of materials. This program performs major functions necessary for controlling an ultrasonic apparatus, analyzing the measurement data generated by the apparatus, and displaying the results of the analysis. Written in the LabVIEW programming language, ULTRA SON is intended to supplant older ultrasonic-testing programs that are difficult to use and that require large computers: ULTRA SON is user-friendly and can be executed on personal computers.

For a given specimen to be characterized, ULTRA SON guides the user by generating an interactive display (part of a LabVIEW "Virtual Instrument") that contains a sequence of buttons and windows through which the user sets the parameters of the sequential measurement, analysis, and display operations pertaining to that specimen. The user provides input via a keyboard, a mouse, or both. The figure presents an example of an ULTRA SON interactive display.

ULTRA SON provides for analog-to-digital conversion at a sampling rate up to ≈1 GHz. Once a set of ultrasonic-echo data for a specimen has been acquired, ULTRA SON processes the data to calculate the ultrasonic properties that are often used to characterize the bulk nonultrasonic physical properties and microstructure of the specimen. These ultrasonic properties include the following:

- The phase velocity and the attenuation coefficient, both as functions of frequency;
- Reflection coefficients;
- Cross-correlation velocity;
- Peak frequencies, bandwidths, durations, rise times, fall times, slew rates, and overshoots of pulses; and
- Magnitude, phase, and power spectra.

In this program, with the exception of power spectra, ultrasonic properties are calculated on the basis of magnitude (as opposed to power) frequency-domain spectra.

ULTRA SON is written for use on a personal computer with a minimum recommended "586 processor operating at a speed of at least 133 MHz and running the Windows 95 or Windows NT4.0 operating system. A Sonix, Inc., STR"81g card (which contains a 1-GHz analog-to-digital converter) and the associated software must be installed in the computer. The user-interface part of ULTRA SON is designed for a video monitor with a resolution of 1,024 × 768 pixels and a size of at least 20 in. (51 cm).

This program was written by Don J. Roth and Wei Cao of **Glenn Research Center.** *Further information is contained in a TSP [see page 1].*

Inquiries concerning rights for the commercial use of this invention should be addressed to NASA Glenn Research Center, Commercial Technology Office, Attn: Steve Fedor, Mail Stop 4–8, 21000 Brookpark Road, Cleveland, Ohio 44135. Refer to LEW-16703.

Parallel 3D EMPIC Algorithm Using Nonorthogonal Grids

This algorithm is suitable for large-scale simulations of plasmas.

NASA's Jet Propulsion Laboratory, Pasadena, California

Electromagnetic particle-in-cell (EMPIC) codes provide a capability for numerically simulating the motions of electrically charged particles in electromagnetic fields, and hence have become standard software tools in plasma physics research. Most existing EMPIC codes are based on the use of orthogonal computational grids (Cartesian or cylindrical). The applicability of such codes is restricted to problems with simple geometries.

A new, three-dimensional (3D) EMPIC algorithm using nonorthogonal grids has been developed recently for parallel supercomputers. The algorithm and a computer code that implements this algorithm can be used to study plasma problems involving complex geometries, such as those related to microwave devices.

One prior EMPIC algorithm using nonorthogonal grids is based on a finite-element approach. The present algorithm and code are based on a finite-volume approach. The major features of the present algorithm are the following:

- The building blocks of computational grids are logically connected, nonorthogonal, deformable hexahedral cells. As a result, grids can be made to accommodate complex geometries for large-scale simulations of plasmas.
- The electromagnetic-field-update phase of the computational cycle is based on a discrete-volume generalization of the standard finite-difference time-domain (FDTD) algorithm; this formulation makes the algorithm simpler than the corresponding finite-element-based algorithm.
- The particle-push phase of the computational cycle involves a hybrid logical/physical-space operation.
- The implementation of this algorithm uses a domain decomposition of a grid and particles that is almost identical to that of a Cartesian grid based EMPIC algorithm.

The combination of features makes it possible to perform 3D large-scale simulations of plasma physics problems involving complex geometries with a very high parallel-computing efficiency (> 98 percent).

This work was done by Joseph Wang, Paulett Liewer, Dimitri Kondrashov, and Steve Karmesin of Caltech for **NASA's Jet Propulsion Laboratory.** *Further information is contained in a TSP [see page 1].*

NPO-20496

BLANK PAGE

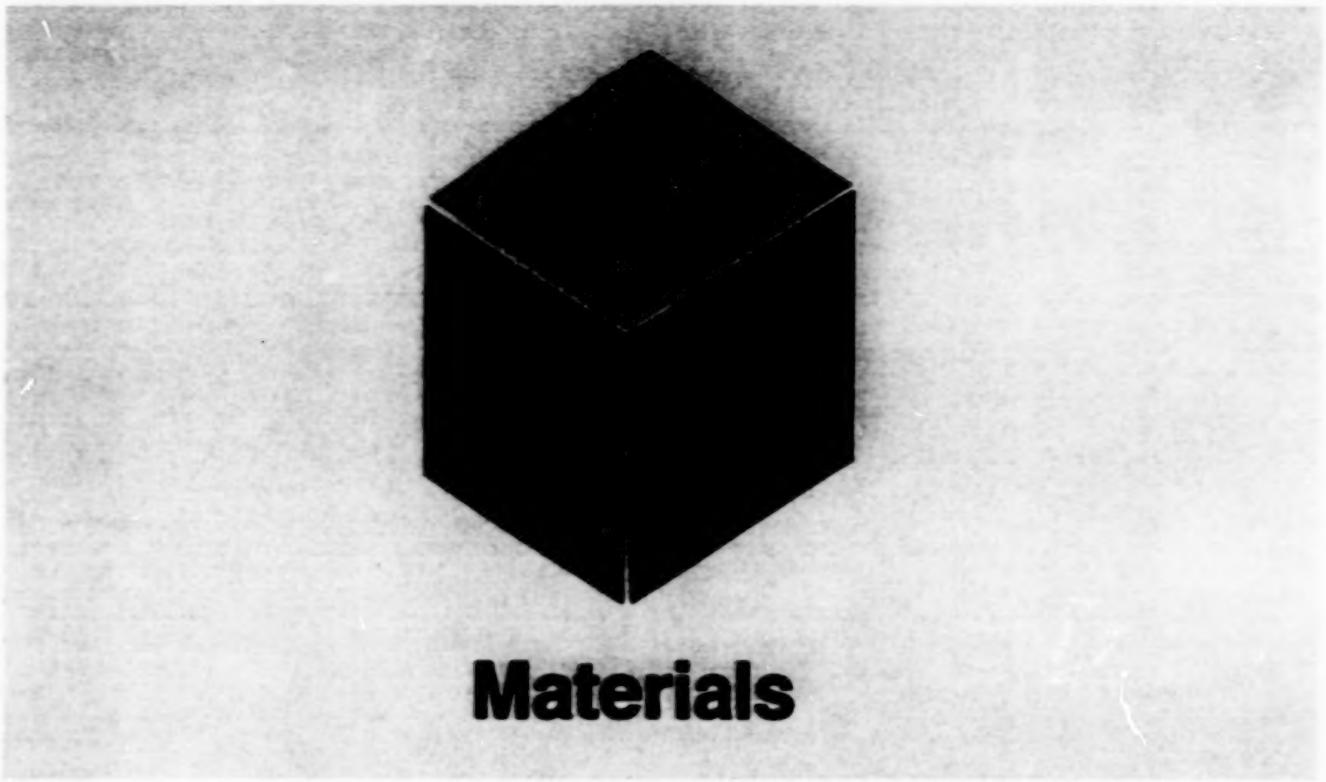

Materials

Hardware, Techniques, and Processes

35 Nonevaporable Getters To Maintain Vacuum in Sealed MEMS
35 Protective Shells for Composite Overwrapped Pressure Vessels
36 Lightweight Reflector Dishes Would Be Made by Spin Casting

BLANK PAGE

Nonevaporable Getters To Maintain Vacuum in Sealed MEMS

These getters would prolong operational lifetimes.

NASA's Jet Propulsion Laboratory, Pasadena, California

Nonevaporable getters have been proposed for use in maintaining vacuum inside hermetically sealed microelectromechanical systems (MEMS) that rely on vacuum for proper operation. A vibratory microgyroscope is an example of such a MEMS. The proposed getters could also be used in such vacuum components as cathode-ray tubes, microwave tubes, conventional electron tubes, plasma display devices, particle accelerators and colliders, vacuum thermal insulation, ultrahigh-vacuum systems for processing semiconductors, x-ray tubes, lamps, and field-emission display devices.

The need for getters arises as follows: Over time, the vacuum inside a sealed MEMS (or inside any other sealed vacuum device, for that matter) is degraded by outgassing of common atmospheric gases and packaging-material vapors from the surfaces of the vacuum chamber, and by diffusion and/or microleaking of these and other gases. Getters are materials that help maintain vacuum by chemically sorbing gases. Getters have been used in vacuum electron devices since the early years of electronic technology, but until now, there has been little systematic effort to incorporate them into MEMS.

The proposed getters would be components of the MEMS vacuum packaging in which they would be installed. They could be fabricated in simple planar shapes or in more complex three-dimensional shapes. They would be made from Zr-Al-Fe, Zr-V-Fe, or other suitable materials (SAES Getters USA Inc., CO, USA). They would be made highly porous to facilitate access of gases and to provide high active surface area for sorption. The getters would be required to be mechanically stable in the sense that they must endure any vibrations or shocks during use and must not shed particles (which could interfere with MEMS functions) at any time during fabrication, activation, or use.

In general, getters must be activated prior to use. Activation is an integral part of the process of fabrication of the device in which a getter is installed. A getter of the proposed type would be handled, installed, and activated according to the following instructions:

1. A getter should be handled only with clean tools or with rubber or plastic gloves, and never with bare hands.
2. A getter could be cleaned by ultrasonic agitation in highly pure isopropyl alcohol for a few seconds, then dried in an oven.
3. For long-term storage, a getter should be placed in a clean, dry environment; e.g., a phosphorus pentoxide or silica gel dessicator or a dry nitrogen atmosphere.
4. Weld the getter into the MEMS package according to the fabrication procedure for the particular MEMS design.
5. Apply a vacuum pump to the MEMS until the pressure in the vacuum chamber in the MEMS is $<10^{-6}$ torr ($<10^{-4}$ Pa).
6. Activate the getter by heating.
   (a) The activation parameters are temperature, time, and method of heating; the amount of time spent at a constant activation temperature is very important.
   (b) The temperature of the getter should be monitored by use of thermocouples, at least until the heating parameters (e.g., heater power and time) that yield the required activation temperature for the required time have been established.
   (c) The rate of heating during activation should be controlled to prevent excessive outgassing.
   (d) Monitor the maximum pressure during activation to obtain an indication of the gas content of the getter.
7. Allow the getter to cool to its test temperature while still pumping.
8. Carefully pinch off and seal the vacuum chamber in the MEMS package.

This work was done by Rajeshuni Ramesham of Caltech for NASA's Jet Propulsion Laboratory. Further information is contained in a TSP [see page 1].
NPO-20617

Protective Shells for Composite Overwrapped Pressure Vessels

These laminated shells are lightweight, inexpensive, and removable.

Lyndon B. Johnson Space Center, Houston, Texas

White Sands Test Facility (WSTF) scientists have developed an energy-absorbing laminated shell that is a prototype of lightweight, inexpensive, and removable covers to shield and otherwise protect carbon-composite overwrapped pressure vessels (COPVs). Although COPVs are superior to metal vessels in strength and weight savings, shielding and other protection are needed because COPVs are highly susceptible to damage by impacts.

The present protective shell is not only an energy-absorbing laminate that can shield a COPV against damage by impacts but is also instrumented with a piezoresistive force sensor that can be configured as an alarm indicator to warn of impacts that exceed a threshold level. Shells like this one will thus prove invaluable not only to spacecraft and launch vehicles but also to manufacturers of composite structures (e.g., pressure vessels, support structures, aerospace surfaces, and life support vessels); moreover, utility may extend to the automotive industry, wherein protective shells for COPVs could protect fuel tanks against ruptures following severe impacts.

Spacecraft and launch-vehicle designers are increasingly storing high-pressure gases and liquids in COPVs. These vessels are fragile and can be easily damaged by being dropped, by rough handling, or by impacts of dropped tools. Ensolite foam has been used until now to provide some measure of protection. But WSTF studies have concluded that Ensolite foam alone affords scant protection against appreciable impacts. Indeed, the experiments have shown that when a COPV is shielded only by Ensolite foam, when an impact occurs at a speed of about 19 m/s, a maximum deflection of 0.156 in.(3.96 mm) takes place at about 7 ms later, and the impact leaves a permanent deformation of 0.015 in. (0.38 mm). In practice, such damage would necessitate replacement of a COPV — a costly proposition and a potentially hazardous practice in space flight. The WSTF test program has also revealed that COPV unprotected except for a layer of Ensolite foam can be severely degraded by an impact at an energy of 35 ft-lbf (47 J). Thus, the WSTF test program has revealed a need for protection better than that afford-

ed by Ensolite foam.

The present energy-absorbing laminated protective shell has been developed to satisfy this need. This shell has several novel features: Aluminum mesh foam is used as an energy-absorbing material to reduce deflection damage; a composite hard shell material is used to absorb indentation energy; and the aforementioned piezoresistive force sensor is used to indicate impacts with energies above 15 ft-lbf (20 J) — the threshold energy level tested by WSTF. (In research and development to advance the design of the shell, the piezoresistive force sensor has also been used as an oscilloscope trigger.)

The laminate comprises four layers, each performing a specific function: (1) a 0.5-in. (12.7-mm)-thick Ensolite foam layer; (2) a 0.05-in. (1.3-mm)-thick composite inner shell; (3) the aluminum mesh foam layer, which is 0.5 in. (12.7 mm) thick; and (4) a 0.375-in. (9.5-mm)-thick composite hard shell. Ensolite foam gives protection against scuffing; the composite inner shell provides a flat, rigid surface on which the aluminum foam rests; the aluminum foam absorbs most of the impact force from compression; and the composite outer shell prevents penetration by sharp objects. The piezoresistive force sensor is embedded between the Ensolite foam and composite inner shell layers.

In a test performed on a COPV protected by this shell, an impact occurred at a speed of about 20 m/s and a maximum deflection of 0.05 in. (1.3 mm) took place at about 6 ms later. No permanent deformation remained after the test. These results demonstrate a significant improvement over a COPV shielded with Ensolite foam alone.

This work was done by Ralph M. Tapphorn and Tim E. Roth of Rockwell Space Operations for **Johnson Space Center.**

MSC-22762

Lightweight Reflector Dishes Would Be Made by Spin Casting

These dishes could be mass-produced cheaply.

NASA's Jet Propulsion Laboratory, Pasadena, California

Lightweight reflector dishes for radio antennas would be mass-produced cheaply by spin casting of polymers, according to a proposal. These reflector dishes were conceived for compact stowage followed by deployment and operation aboard spacecraft, but might also be useful on Earth in applications in which there are requirements for extremely light weight and stowability but not for highly precise reflector shape.

The spin-cast reflector dishes would be thin and flexible, and thus foldable for compact stowage. In some applications, it could be desirable to rigidize the dishes after deployment. This could be done, for example, by making dishes of an ultraviolet-curable polymer and exposing them to ultraviolet light (e.g., as part of sunlight) immediately after deployment. Alternatively, dishes could be made of a material with a glass-transition temperature above that of the deployment environment; after deployment, these dishes would be allowed to cool naturally, so that they would be rigidized by the rubber-to-glass transition.

This work was done by Celeste Satter of Caltech and Dan Marker of the Directed Energy Directorate, Air Force Research Laboratory, for **NASA's Jet Propulsion Laboratory.** *Further information is contained in a TSP [see page 1].*

NPO-20548

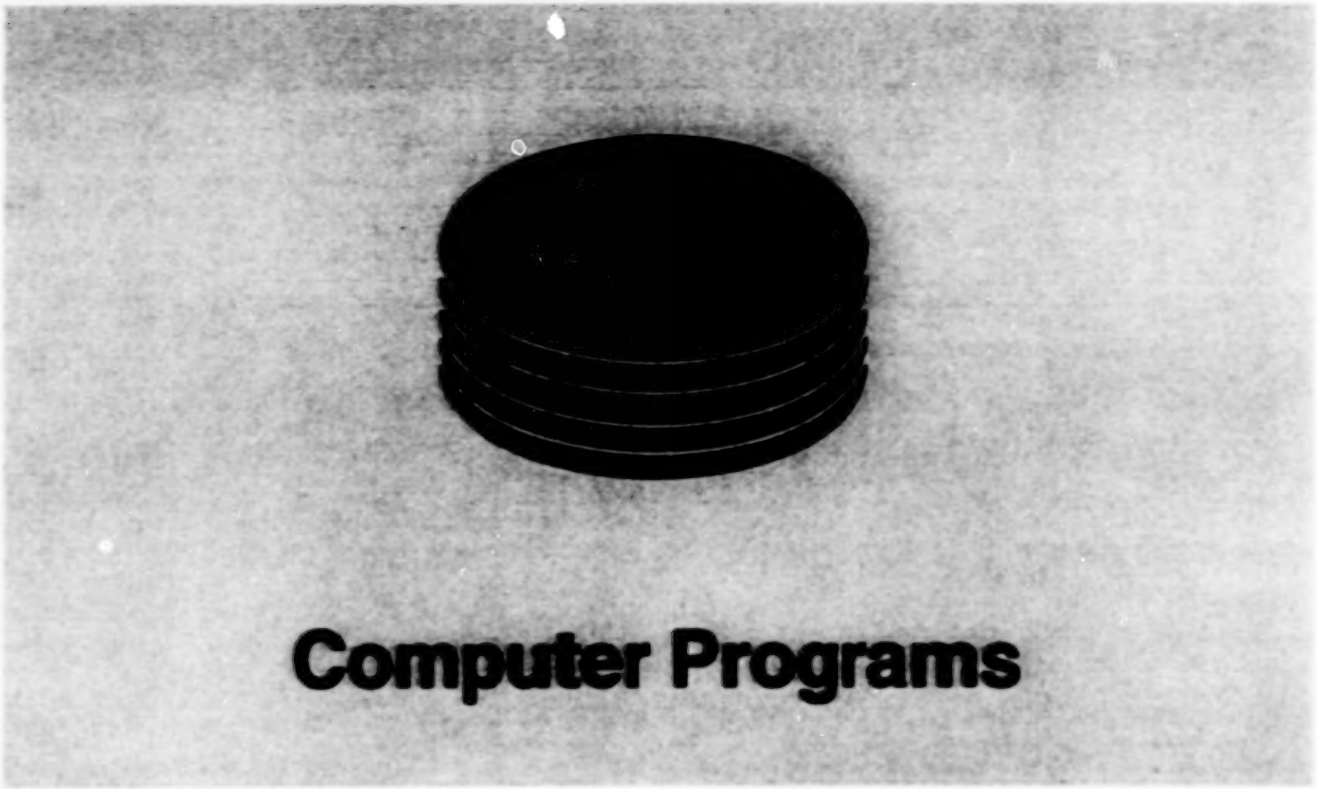

Computer Programs

Mechanics

39 Monocoque Tank Analysis Spreadsheet System, Version 2.0

Mathematics and Information Sciences

39 Automated Planning and Scheduling for a Robotic Vehicle

BLANK PAGE

Mechanics

Monocoque Tank Analysis Spreadsheet System, Version 2.0

This program can be used to design both pressurized and nonpressurized tanks and conical structures.

The Monocoque Tank Analysis Spreadsheet System (MONTASS) computer program is an integrated software system that incorporates Microsoft Excel worksheet software and Visual BASIC software. MONTASS was developed to enable rapid analysis and preliminary design of structural domes and truncated sections of cones.

MONTASS performs both design and analysis functions by (1) calculating the minimum skin thicknesses needed to enable analyzed and/or designed components to withstand design temperatures and loads (as in a proof test), and then (2) running stress and buckling analyses under operational temperatures and loads. Although MONTASS was developed to analyze monocoque propellant tanks, it can also be used to analyze nonpressurized conical structures.

MONTASS can be run easily from a user-friendly, three-page interface worksheet that controls a propellant-tank-analysis software subsystem. Two other visible worksheets present information on properties of materials as functions of temperature and a table of stored fluids and densities. The user can customize the data on both of these worksheets. The MONTASS system also includes six component worksheets and two Visual BASIC functions that are ordinarily hidden from view but can easily be viewed by following directions given on the interface sheet.

Design and analysis inputs include shapes and sizes, minimum allowable skin thicknesses (constraints imposed by manufacturing or fracture mechanics), properties of fluids, safety factors, a choice of the max principle or the von Mises failure criterion, loads, and temperatures. Properties of materials are interpolated from the data base for the input temperatures specified by the user. The user can also choose to design a dome with either a constant or a tapered skin-thickness distribution.

The primary design data products from MONTASS are internal volumes, skin thicknesses, and a summary of masses. Using these data, MONTASS then performs a stress analysis for all components and a buckling analysis for truncated section of a cone. Analysis load sets can include bending moments, axial forces, ullage pressures, hydrostatic pressures, longitudinal acceleration, and rotations. Analysis data products from MONTASS are a summary of radial and vertical deflections, material-failure margins of safety for all components, and buckling margins of safety for the truncated section of a cone. If the analysis has shown that a tank can be expected to fail in buckling, then MONTASS also calculates the pressure needed to stabilize the tank.

Stand-alone components are included in MONTASS to provide users the option to run the MONTASS computational tools without using the interface that is integral to the MONTASS system. An additional Excel worksheet calculates the skin thickness of a monocoque cylinder that yields the same moment of inertia as that of a cylinder of a given thickness reinforced with integral T stiffeners.

MONTASS was developed as a Microsoft Excel v5.0a workbook program on a Power Macintosh computer. MONTASS has also been implemented on '486- and '586-class personal computers using Microsoft Excel v7.0a for Windows 95. The standard distribution medium for MONTASS is a 3.5-in. (8.89-cm), 1.44MB diskette in MS-DOS format. Power Macintosh computers can read MS-DOS-format diskettes; however, a Macintosh-formatted diskette can be made available if necessary. The documentation is available on the spreadsheets only. MONTASS was developed in 1998. The program is a copyrighted work with all copyright vested in NASA.

This program was written by P. L. Luz of **Marshall Space Flight Center.**

Inquiries concerning this program should be addressed to Larry Gagliano at the Center Software Release Authority at Marshall Space Flight Center (telephone 205-544-7175).

MFS-31223

Mathematics and Information Sciences

Automated Planning and Scheduling for a Robotic Vehicle

A software system generates sequences of commands for the operation of a robotic vehicle. The system was adapted to control Rocky 7, a semiautonomous instrumented vehicle of the "rover" type used in scientific exploration of Mars. The software system was developed by integrating two software systems reported in previous *NASA Tech Briefs* articles: Web Interface for Telescience (WITS) and Automated Scheduling and Planning Environment (ASPEN). WITS provides a high-level graphical interface, through which a user can specify scientific activities and locations by referencing to images of the environment of the robotic vehicle. ASPEN accepts the scientific goals specified by use of WITS, then reasons about the low-level activities and resources needed to attain these goals. ASPEN then generates an executable sequence of commands to perform the requested scientific observations; these include commands to travel to and/or between specified locations in order to arrive at locations where observations are to be performed. In generating the commands, ASPEN enforces flight rules and detects and resolves conflicts over resources by reordering scientific observations, adding required activities, and/or deleting low-priority observations. The further development of this software system is likely to include installation of the software in the rover itself to enable the rover to schedule its own activities, and thus to behave more autonomously.

This program was written by Gregg Rabideau, Steve Chien, Paul Backes, Gene Chalfant, and Tara Estlin of Caltech and Kam Tso of IA Tech, Inc., for **NASA's Jet Propulsion Laboratory.** *Further information is contained in a TSP [see page 1].*

This software is available for commercial licensing. Please contact Don Hart of the California Institute of Technology at (818) 393-3425. Refer to NPO-20574.

BLANK PAGE

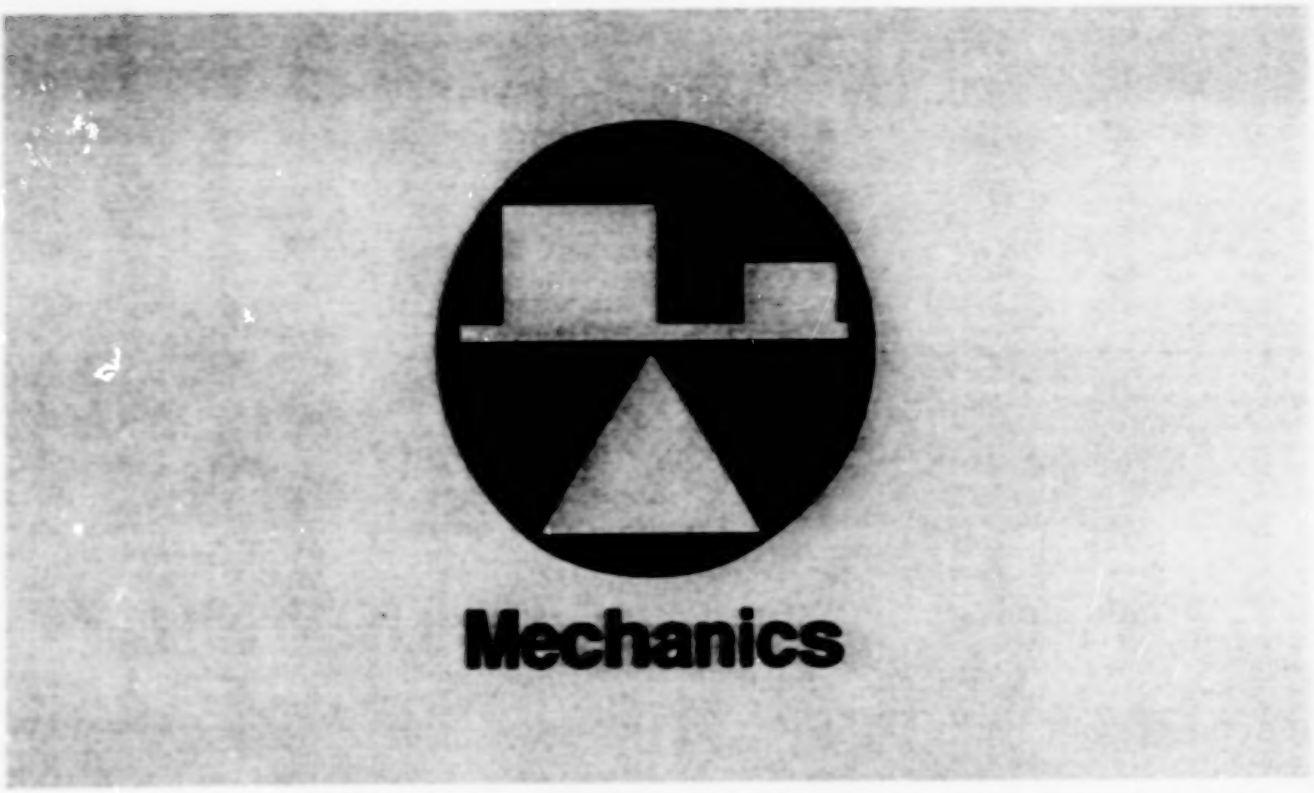

Hardware, Techniques, and Processes

43 Spherical-Coordinates Encoder Module

BLANK PAGE

Spherical-Coordinates Encoder Module

Three-dimensional offsets can be measured with ease.

John F. Kennedy Space Center, Florida

The spherical-coordinates encoder module (SCEM) is a relatively simple and inexpensive electromechanical apparatus for quickly and easily measuring three-dimensional offsets between objects at distances of the order of a few feet (≈1 m). The SCEM was developed specifically for measuring offsets between spacecraft payload trunnions and trunnion supports during ground-based payload-transfer operations; it could also be readily used, for example, to measure offsets to guide the maneuvering of large objects during the assembly of heavy machinery or structures. The SCEM eliminates the need for time-consuming, tedious, error-prone measurements by use of such tools as scales, tapes, and protractors, followed by equally tedious and error-prone manual calculations, manual recording of data, and verbal communication of data.

The SCEM is so named because the raw measurement data that it produces are essentially spherical coordinates. The SCEM includes a mechanical unit, part of which rotates about a nominally vertical and a nominally horizontal coordinate axis (see top part of figure). The coordinate axes are defined by mating of the nominally stationary base of the mechanical unit with a mounting bracket on the first of the two objects, the offsets between which one seeks to measure. The mechanical unit contains a spring-loaded reel, on which is wound a 0.25-in. (6.35-mm) timing belt. Two optical encoders measure the rotations about the vertical and horizontal coordinate axes (azimuth and elevation angles, respectively). A third optical encoder measures the rotation of the reel for determining the length of timing belt pulled off the reel and thus the radius from the origin of coordinates to the tip of the outstretched belt.

To perform a measurement, a technician simply pulls the wire from the wheel and places the tip of the wire on the point of interest on the second of the two objects, the offset between which one seeks to measure (see bottom part of figure). The spring tension keeps the belt straight and pulls the rotating part of the mechanical unit into an orientation along the offset vector of interest. Thus, the azimuth and elevation optical encoders provide data on the offset direction, while the reel optical encoder provides data on the offset radius.

The outputs of the optical encoders are fed to a portable computer, which is programmed with data-collection and user-interface software. The software includes components that implement the trigonometric formulas of transformation from spherical to Cartesian coordinates. The offset in Cartesian coordinates is displayed on the computer screen.

The mechanical unit fits within a 7.5-in. (19-cm) cube. At a radial offset of 18 in. (45.7 cm), the SCEM can measure azimuth angles from 0° to 340°, accurate to within an 0.30°; and it can measure elevation angles from 10° to 100°, accurate to within an average of 0.300°. The SCEM measures radius to within an average of 0.005 in. (0.13 mm). The basic SCEM can be expanded to include as many as 18 to 20 mechanical units communicating with a single computer. The information displayed on the computer screen can be updated at a rate of four times per second.

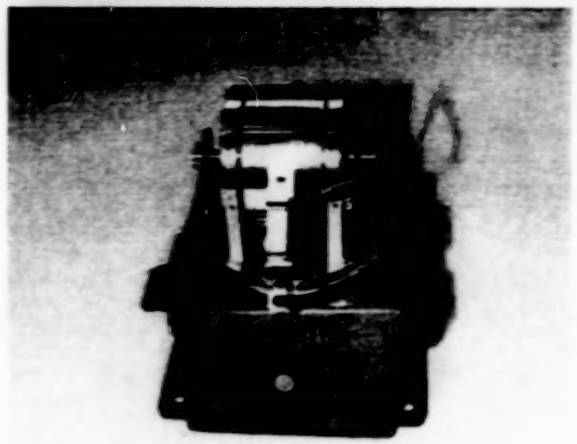

SCEM Mechanical Unit

SCEM IN USE

The SCEM is an electromechanical apparatus for measuring three-dimensional offsets. To measure the offset of a nearby object, one simply stretches a spring-tensioned wire from the unit to the object.

This work was done by Eduardo Lopez Del Castillo and Felix A. Soto Toro of **Kennedy Space Center**. *Further information is contained in a TSP [see page 1].*

Inquiries concerning rights for the commercial use of this invention should be addressed to the Technology Programs and Commercialization Office, Kennedy Space Center, (407) 867-6373. Refer to KSC-11973.

BLANK PAGE

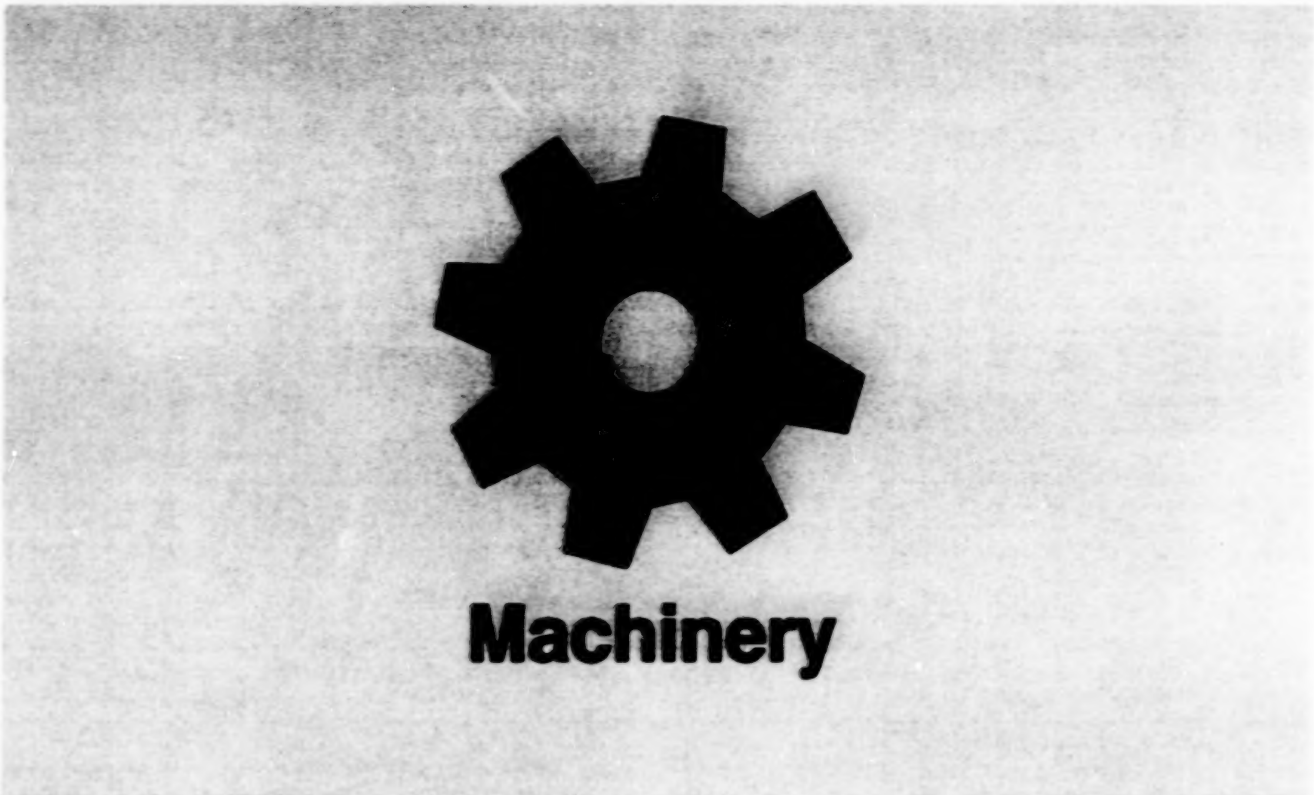

Machinery

Hardware, Techniques, and Processes

47 MEMICA: a Concept for Reflecting Remote-Manipulator Forces
48 Adaptive Variable Bias Control for Magnetic Bearings

BLANK PAGE

MEMICA: a Concept for Reflecting Remote-Manipulator Forces

Damping or resistance would be controlled electronically.

NASA's Jet Propulsion Laboratory, Pasadena, California

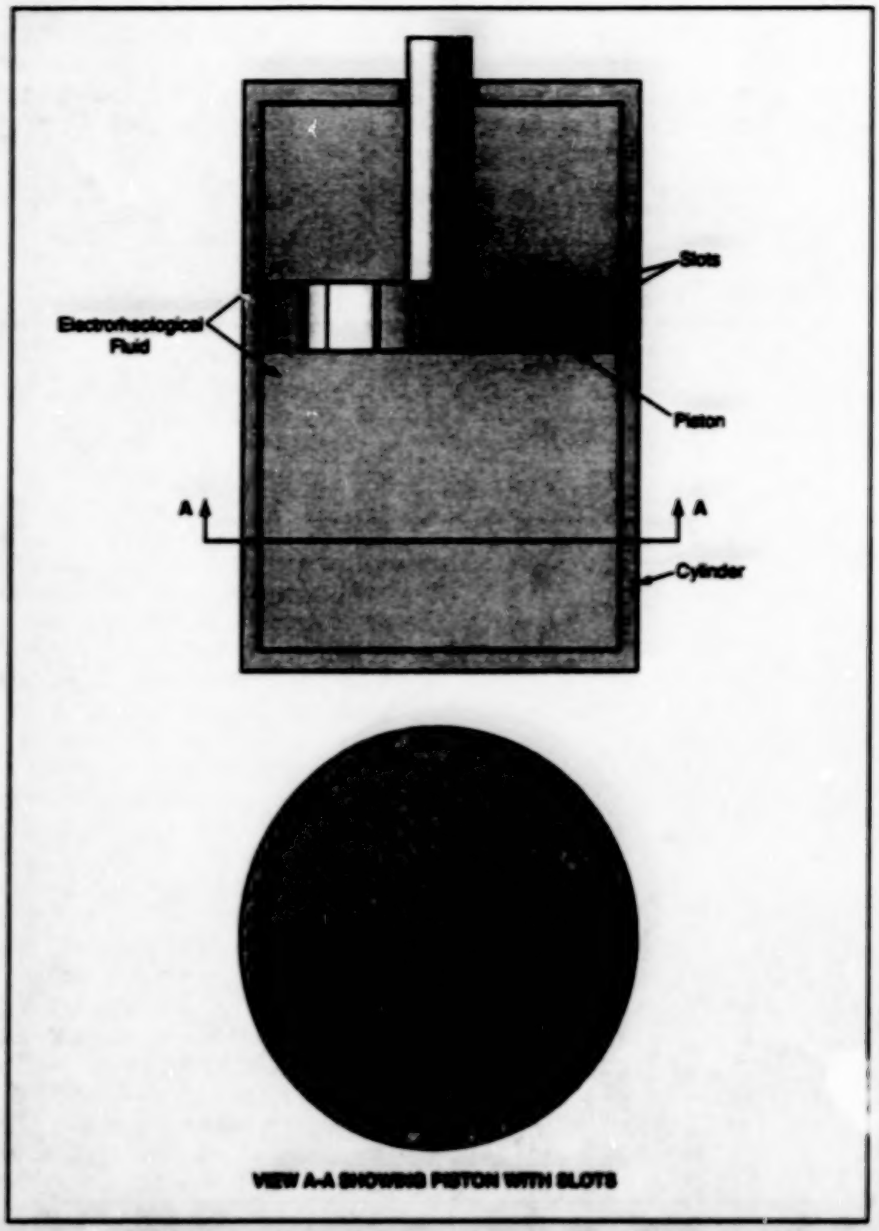

Figure 1. An ECS Device would resist elongation or shortening with a stiffness that would depend on the voltage applied across the electrorheological fluid flowing past the piston in the slots.

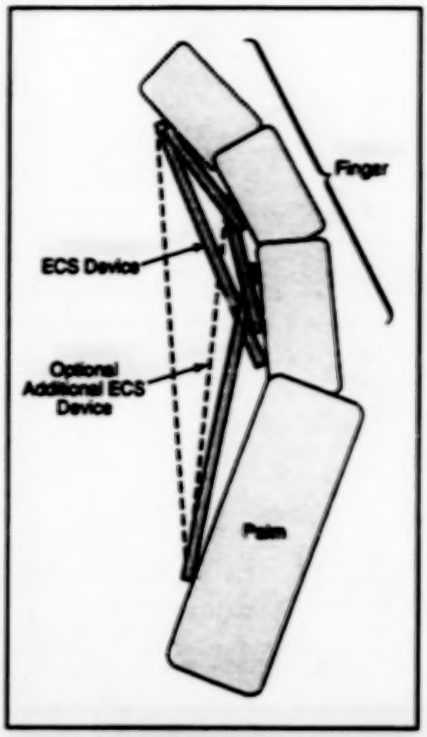

Figure 2. ECS Devices would mirror the stiffness distribution at the corresponding locations on a remote robot finger.

The term "mechanical mirroring using controlled stiffness and actuators" ("MEMICA") denotes a developmental concept for reflecting contact forces, displacements, mechanical damping, and temperature from the hand of a remote robotic manipulator back to the hand of a human operator who controls the manipulator. The MEMICA concept is expected to result in improvements in the remote control of robots in hostile environments, and may make it possible to perform remote surgery. The concept could also be applied to providing tactile sensations of objects in computationally simulated environments ("virtual reality") and to exercise machines. The MEMICA concept could be implemented by means of various operator interfaces (e.g., joysticks, knobs, or gloves). The purpose of developing MEMICA is to enable a human operator to feel, more realistically, the stiffness, temperature, vibration, and other tactile characteristics of objects to be remotely or virtually manipulated, thereby enhancing dexterity in remote manipulation or increasing the degree of perceived realism in a simulated environment.

In a typical implementation of MEMICA for controlling a remote anthropomorphic robot hand, the robot hand would be equipped with actuators to generate the desired motions and forces, and would be instrumented with contact-force, temperature, and position sensors. The operator interface would be a glove instrumented with (1) mechanical actuators to reflect the displacements and the reaction (contact) forces; (2) operator-hand-action sensors, the outputs of which would be processed to generate commands for controlling the robot hand; and (3) thermoelectric heater/cooler units to provide thermal feedback from the robot hand. Thus, in a sense, the glove and the robot hand would mirror each other.

One of the major features that distinguishes the MEMICA concept from other concepts of force-reflecting robotic control is the proposed use of electrically controlled stiffness (E[illegible]) devices at selected locations on the instrumented glove to mirror the forces of resistance to motion at the corresponding locations on the robot hand. An ECS (see Figure 1) would include a piston in a cylinder filled with an electrorheological fluid. Slots on the cylindrical piston surface would allow the liquid to flow past the piston during displacement of the pis-

ton. The slots would be lined with electrodes. The slots and electrodes would be dimensioned so that by application of voltage over a suitable range, the viscosity of the fluid, and thus the force of resistance of the piston to displacement, could be controlled over a desired range. Each finger of the glove would be equipped with ECS devices (see Figure 2) to generate reaction forces to apply the required force feedback to the operator's finger. The ECS part of the MEMICA concept is also potentially applicable to active damping of vibrations in "smart" structures.

While ECS devices could reflect resistance to motion, they could not actively reflect forces and displacements; that is, they could not reflect the action of something pulling or pushing on the robot hand and could not reflect vibrations. For active reflection of forces and displacements (including vibrations), it would be necessary to equip the glove with other actuators. Hydraulic, pneumatic, and shape memory alloy linear actuators have been considered for this purpose. An alternative linear actuator that might be used for this purpose would be, essentially, a motor-driven variant of a common curvature-stiffened metal tape measure.

This work was done by Yoseph Bar-Cohen and Benjamin Dolgin of Caltech and Charles Pfeiffer and Constantinos Mavroidis of Rutgers University for **NASA's Jet Propulsion Laboratory**. *Further information is contained in a TSP [see page 1].*
NPO-20642

Adaptive Variable Bias Control for Magnetic Bearings

Power consumption is reduced, without sacrificing performance.

John H. Glenn Research Center, Cleveland, Ohio

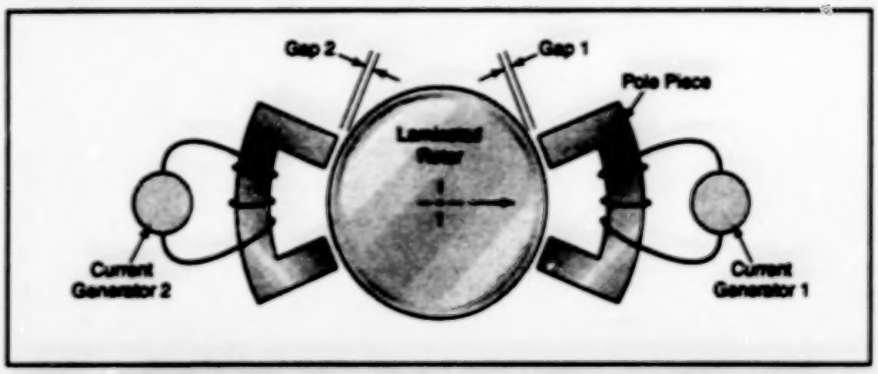

Figure 1. A Magnetic Bearing utilizes magnetic forces to levitate a rotor without rotor/stator contact. For the sake of simplicity, electromagnets are shown on only one axis; to function properly, a bearing must include electromagnets on at least two axes.

Figure 2. This Eight-Pole Magnetic-Bearing Test Apparatus was used in experiments on AVBC.

Adaptive variable bias control (AVBC) is an improved technique for controlling the currents supplied to the electromagnets in magnetic bearings. In AVBC, the bias currents are varied in such a way as to reduce overall power consumption.

In a magnetic bearing (see Figure 1), the magnetic forces depend nonlinearly upon the currents flowing in the electromagnet coils and on the distances between the rotor and the stator poles. Because the magnetic forces are attractive only and decrease with increasing distances, magnetic bearings are open-loop unstable and, consequently, closed-loop control is necessary for stable operation. A conventional control scheme for a magnetic bearing includes the decomposition of the total current into a constant bias component and a varying command component in order to linearize the relationship between the command component and the force delivered by the bearing. Usually, such classical feedback control techniques as proportional-derivative (PD) or proportional-integral-derivative (PID) are used.

Bias currents give rise to consumption of power, even when no loads are supported by the bearings. AVBC was developed as an alternative control technique in which bias currents, and thus power-consumption levels, are reduced. Another, closely related benefit of reductions in bias currents is reduction in overall generation and dissipation of heat (including eddy-current and hysteretic heating of rotors).

AVBC is based on the conventional bias method, but departs from that method according to the principle that by varying the bias current adaptively as needed, the power consumption in a bearing can be reduced while producing the desired force and maintaining the linearization afforded by using bias. The main static influence in changing the bias current is to change the static stiffness of the bearing. Dynamically, changing the bias current exerts two effects: the control laws depend on bias, and as the bias changes, the force-slew-rate limit changes. Inasmuch as there are many possible ways to vary the bias, adaptive control is introduced. Adaptive control in this appli-

cation entails monitoring the operation of the magnetic bearing and determining, from the information thus acquired, the best setting for the bias current.

In this approach, the bias setting is not based on typical parameter estimation; instead, it is based on the commanded current. More specifically, the adaptation law is that the bias current is required to equal the average of the amplitude of the command current over a suitable interval of time. The net result is that an AVBC controller is primarily a PD controller with (1) a bias current that is varied and is usually less than it would be in an equivalent conventional controller and (2) a control gain that varies slowly with time and with the bias current. Theoretical calculations and experimentation (see Figure 2) have shown that AVBC is nominally stable and that in comparison with conventional bias control, AVBC yields reduced power consumption and comparable control performance.

This work was done by Dexter Johnson and Gerald V. Brown of **Glenn Research Center** *and Daniel J. Inman of Virginia Polytechnic Institute and State University. Further information is contained in a TSP [see page 1].*

Inquiries concerning rights for the commercial use of this invention should be addressed to NASA Glenn Research Center, Commercial Technology Office, Attn: Steve Fedor, Mail Stop 4–8, 21000 Brookpark Road, Cleveland, Ohio 44135. Refer to LEW-16748.

BLANK PAGE

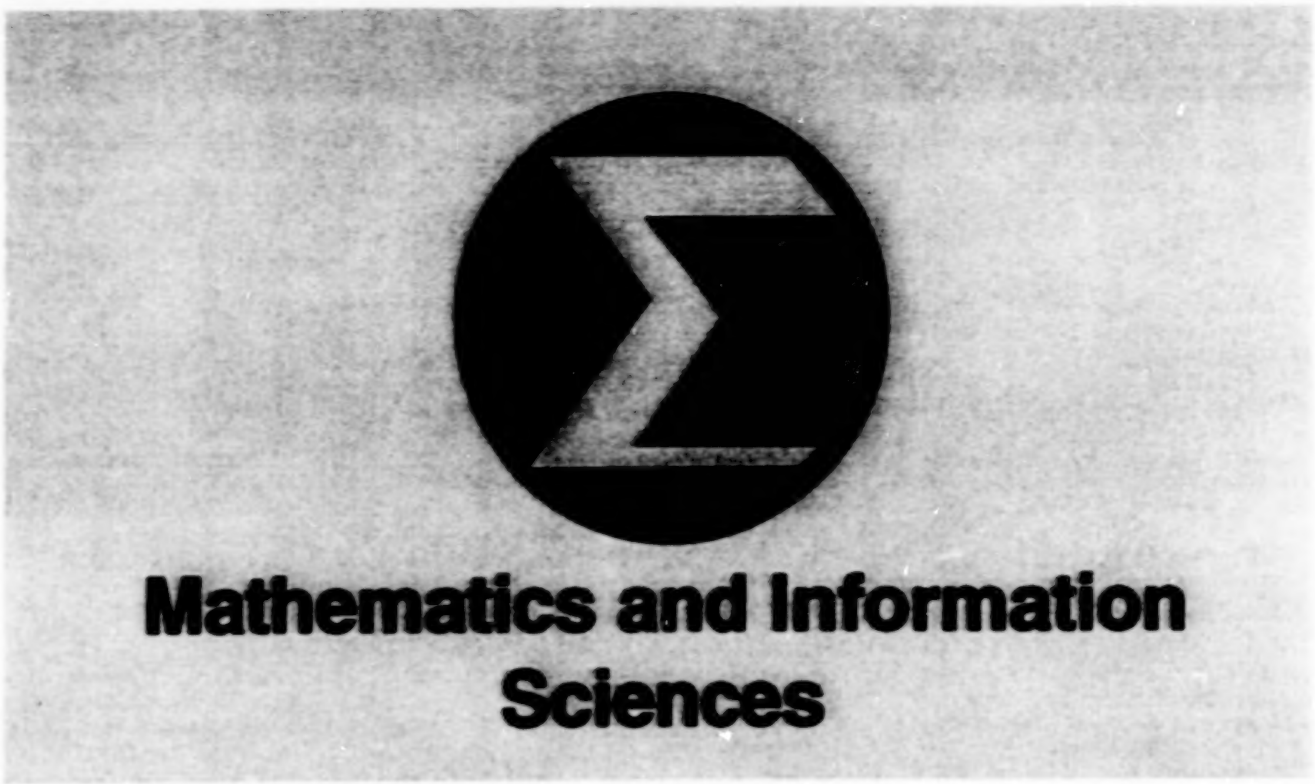

Mathematics and Information Sciences

Hardware, Techniques, and Processes

53 Parameterizing Shape Perturbations for Multidisciplinary Design Optimization
53 Software for Monitoring Remote Systems and Executing Plans
54 Adaptive Filtering of SAR Interferograms

BLANK PAGE

Parameterizing Shape Perturbations for Multidisciplinary Design Optimization

Shapes are deformed by use of soft-objects animation algorithms.

Langley Research Center, Hampton, Virginia

A recently developed method of parameterizing complex shapes that one seeks to optimize differs from prior such methods in two major respects: (1) instead of entirely parameterizing the shapes, one parameterizes only shape perturbations (deformations of initial or baseline shapes) and (2) the deformations are computed by soft-objects animation (SOA) algorithms commonly used in computer graphics. This method is suitable for multidisciplinary design-optimization processes, in which shapes of structures are optimized along with other aspects of design (e.g., aerodynamics). This method can be applied, for example, to the shapes of both exterior aerodynamic surfaces and internal structural components of aircraft.

For example, in the case of an airplane wing (see figure), one starts with a known wing design and seeks to improve the performance of the wing by applying numerical optimization techniques to perturbed wing shapes. Small changes in the shape of a wing can engender substantial changes in aerodynamic performance; as a result, the perturbations between a baseline and an optimized wing design are typically very small.

Baseline and Deformed Planforms of a transport airplane are analyzed in a design-optimization process. Deformations can be represented with computational efficiency by use of SOA algorithms.

Perturbations of a wing shape can readily be expressed as changes in thickness, camber, twist, dihedral angle, shear, and planform; this fact affords a computational advantage in that fewer parameters are needed to express such changes than are needed to describe the wing shape in its full complexity.

SOA algorithms have been chosen for this method because they are powerful computational tools for modifying shapes. In particular, SOA algorithms are suitable for deforming models represented by either sets of polygons or sets of parametric curves and surfaces. The SOA algorithms treat the models as though they were made of rubber that can be twisted, bent, tapered, compressed, or expanded, while retaining their initial topologies. In this respect, SOA algorithms are ideal for parameterizing airplane models that have external skins as well as internal components like spars and fuel tanks. The SOA algorithms relate vertices of the computational grid of an analysis model to a small number of design variables. Consequently, the SOA algorithms can serve as part of the basis of an efficient shape-optimization technique.

This work was done by Jamshid A. Samareh of Langley Research Center. Further information is contained in a TSP [see page 1].
L-17841

Software for Monitoring Remote Systems and Executing Plans

Advantages over predecessor software include enhanced capabilities and greater portability and maintainability.

Goddard Space Flight Center, Greenbelt, Maryland

The Knowledge Server Tools (KST) computer program comprises a distributed set of software tools for monitoring remote systems. Part of KST implements a knowledge server for monitoring the status of a remote system (e.g., a computer-controlled instrumentation system, a robot, or a spacecraft). Another part of KST executes plans. KST was developed to replace older software that was difficult to use, less capable, and less portable.

The tools (the components of KST) are written in freeware Practical Extraction and Report Language (PERL) and communicate with each other via Unix sockets. The components of KST are the following:

- DSI (Data Server Interface) serves as a bridge between external data and KST. DSI loads data and makes them available for KST clients via the PIEKS tool described next.
- PIEKS (PERL Inference Engine Knowledge Server) connects to DSI to get current data whenever it is requested by a client to make an inference. PIEKS includes PIE, which is a frame-based, backward-chaining inference engine. The knowledge representation (frames) in PIE is a natural one to represent model-based reasoning because frames can be organized into hierarchies. PIEKS receives new data, data set by the client, or inferred data. Inferred data are returned if there exists a knowledge-base frame that describes the rule that defines the inferred data. When this is the case, the rule is evaluated and appended to the value of the inferred data. Clients for PIEKS are the APE and HSMON tools described below.
- CCLS (Centroid Classifier Server) connects to DSI to get current data whenever it is requested by a client to classify data. CCLS returns "OK" or the name of the group, the centroid of which is closest to the current normalized data. CCLS can be used to classify data in a way that some case-based systems do. CCLS can be used in conjunction with PIEKS and with APE (described next) to solve problems that require the capabilities of all three of these tools.
- APE (A Plan Executor) is a frame-based hierarchical plan executor. APE connects to PIEKS to set its parameter data and to check the constraints (preconditions and postconditions) of activities. APE also connects to APEMON (which is described next) to highlight the activities that are currently being executed. The knowledge representation in APE separates plans, activity strategy, and constraint checking into three simpler and more flexible files. The same constraints can be used in different activities, and the same activities can be

used in different plans. APE plans can also be nested to any level.

- APEMON (Ape Monitor) highlights buttons with activity names that represent the plan being executed.
- DMON (Data Monitor) connects to PIEKS and plots values of data in real time. Because DMON connects to PIEKS, it can also plot values of inferred data in real time.
- HSMON (Health and Safety Monitor) connects to PIEKS and simply returns the value of a goal defined by PE every N seconds. HSMON may evolve into a tool that returns such information as statuses of all subsystems of the system to be monitored.
- HSDOC (Health and Safety Doctor) connects to PIEKS and launches APE whenever a problem that can be solved easily is identified.
- CCLMON (Centroid Classifier H&S Monitor) connects to CCLS and simply displays the value returned by CCLS.
- CCLHSDOC (Centroid Classifier H&S Doctor) is similar to HSDOC but connects to CCLS instead of PIEKS to classify problems and then launch APE to solve the problems.

The knowledge-server concept greatly enhances the power of this set of tools. By connecting to a knowledge server, a client can obtain raw data, inferred data, and user data (data set by the client). Because all of the tools are written in freeware PERL, the software should be highly maintainable. Because all the tools communicate via sockets, each tool can run on a separate workstation.

This work was done by David R. McLean of AlliedSignal Technical Services Corp. for **Goddard Space Flight Center.** *Further information is contained in a TSP* *[see page 1].*

GSC-14137

Adaptive Filtering of SAR Interferograms

Improves the performance of subsequent phase-unwrapping.

NASA's Jet Propulsion Laboratory, Pasadena, California

An algorithm for filtering synthetic-aperture-radar (SAR) interferograms has been developed which substantially improves the performance of subsequent phase-unwrapping. It accomplishes this task by filtering the interferogram strongly in areas where the scene contains little detail, and weakly where the scene contains much detail. The filter is adaptive in that the amount of filtering is scene dependent.

The interferogram is divided into many small, overlapping patches. Each patch is Fourier transformed in two dimensions. The magnitude of the resulting spectrum is then raised to a user-selected power. An exponent of 1 yields no filtering at all; 2 produces heavy filtering. The patches are then transformed back and accumulated through a rectangular, pyramidal window, which reduces edge effects. It is helpful to normalize the total power of each patch in order to prevent radar-bright areas from unduly influencing their neighbors.

The filter is effective in removing residues, the bane of phase-unwrapping, where the phase is not changing rapidly. However, where the phase does change rapidly, or is noisy, no filtering is applied. This effect prevents phase-unwrapping from occurring where the data does not warrant it.

This work was done by Charles Werner and Richard Goldstein of Caltech for **NASA's Jet Propulsion Laboratory.** *Further information is contained in a TSP* *[see page 1].*

NPO-20440

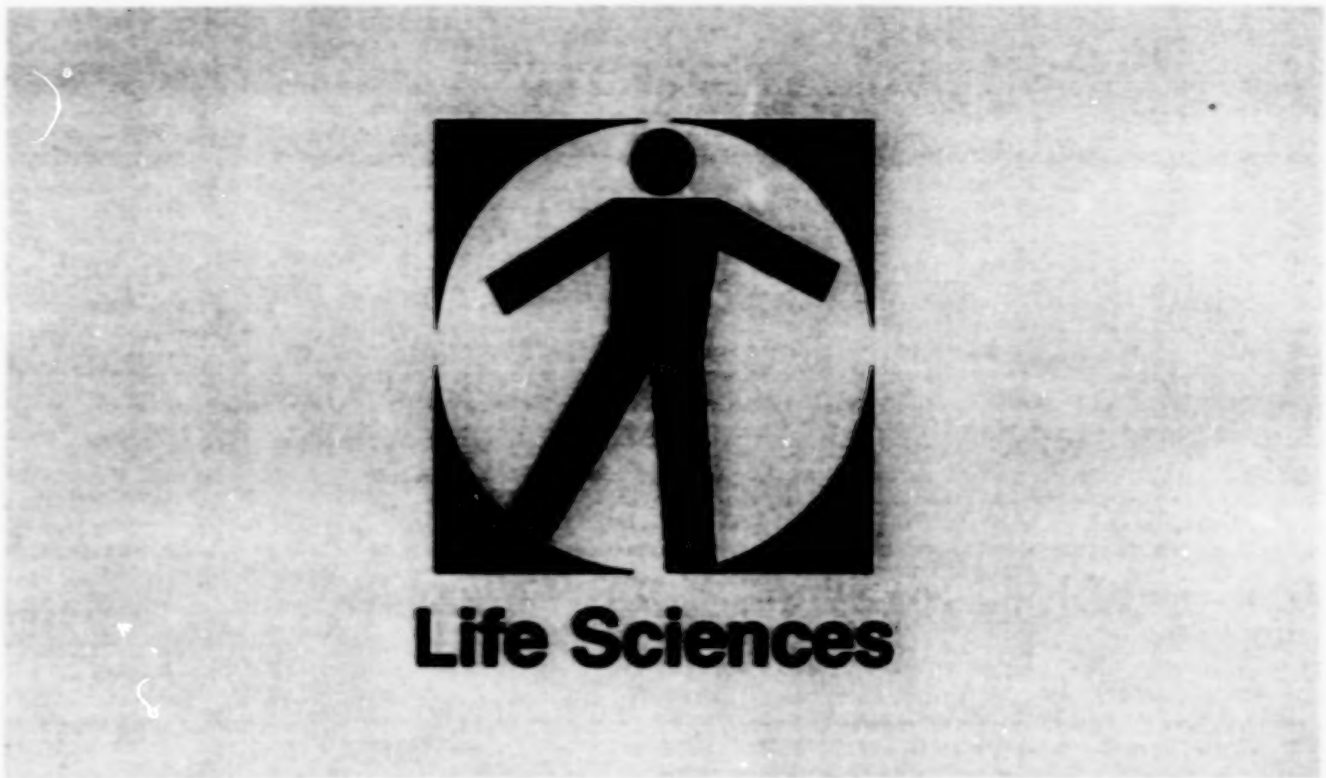

Hardware, Techniques, and Processes

57 Wearable Sensor Patches for Physiological Monitoring
57 Improved Sensor Pills for Physiological Monitoring
58 Urine-Sample-Collection Device for Use on the Space Shuttle

BLANK PAGE

Wearable Sensor Patches for Physiological Monitoring

Noninvasive sensors resembling adhesive bandages would be interrogated by nearby hand-held units.

NASA's Jet Propulsion Laboratory, Pasadena, California

Wearable sensor patches — miniature biotelemetric units — have been proposed for use in measuring temperature, heart rate, blood pressure, and possibly other physiological parameters. The sensor patches would be small and could be mass-produced inexpensively by use of state-of-the-art techniques for batch fabrication of integrated circuits and microelectromechanical systems.

Each patch would be no larger than a few centimeters on a side — comparable in size to an ordinary adhesive bandage. The patch could even be held on the wearer's skin by the same adhesive as that used on bandages. The patch (see figure) would contain a noninvasive microelectromechanical sensor integrated with electronic circuitry that would process the sensor output and transmit a radio signal modulated by the processed sensor output.

The patch would not contain a battery. Instead, the patch would contain a circuit for extracting power from an incident radio beam that would be present during readout. For readout, a hand-held radio transceiver would be positioned near the patch; the transceiver would transmit the radio beam to supply power to the patch circuitry and would receive the modulated radio signal transmitted from the patch.

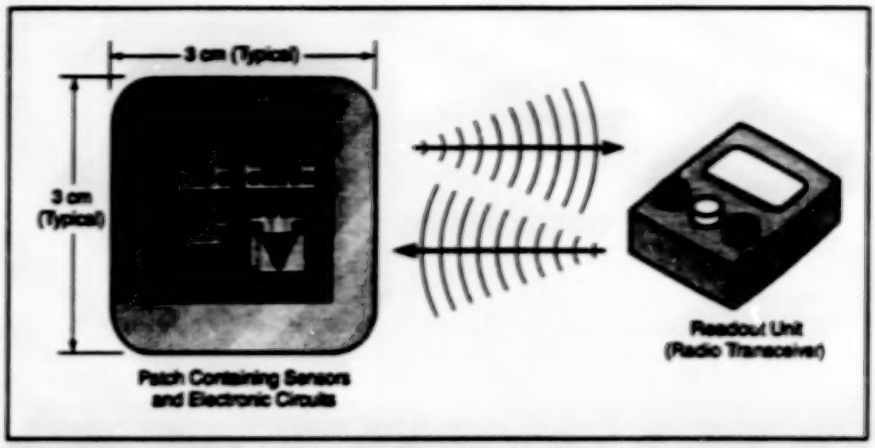

Microelectromechanical Sensors and Electronic Circuits for radio telemetry would be contained in a small patch worn on the skin. A nearby hand-held radio transceiver would provide radio-frequency excitation to energize the circuits and would receive the sensor-readout radio signal from the patch.

This work was done by Gisela Lin and Willem Tang of Caltech for NASA's Jet Propulsion Laboratory. Further information is contained in a TSP [see page 1].

In accordance with Public Law 96-517, the contractor has elected to retain title to this invention. Inquiries concerning rights for its commercial use should be addressed to

Technology Reporting Office
JPL
Mail Stop 122-116
4800 Oak Grove Drive
Pasadena, CA 91109
(818) 354-2240

Refer to NPO-20651, volume and number of this NASA Tech Briefs issue, and the page number.

Improved Sensor Pills for Physiological Monitoring

These pills would measure temperature and sense the presence of blood, bacteria, and chemicals.

NASA's Jet Propulsion Laboratory, Pasadena, California

Improved miniature biotelemetric units resembling large pills have been proposed for use in physiological monitoring of the gastrointestinal tract. The broad principles of design, operation, and inexpensive mass production of these sensor pills would be the same as those of the sensor patches described in the preceding article. Of course, the details of design and operation would differ because the patches and pills would be used in different locations and would sense different phenomena.

A sensor pill would be swallowed and would pass through the gastrointestinal tract in about 24 hours. Like the sensor patches described in the preceding article and like some sensor pills now available commercially, a sensor pill of the proposed type would emit a radio signal that would convey its sensor readings to an exterior monitor. Like some other commercially available sensor pills, the proposed sensor pills could include reservoirs of drugs and actuators to deliver the drugs to designated sites.

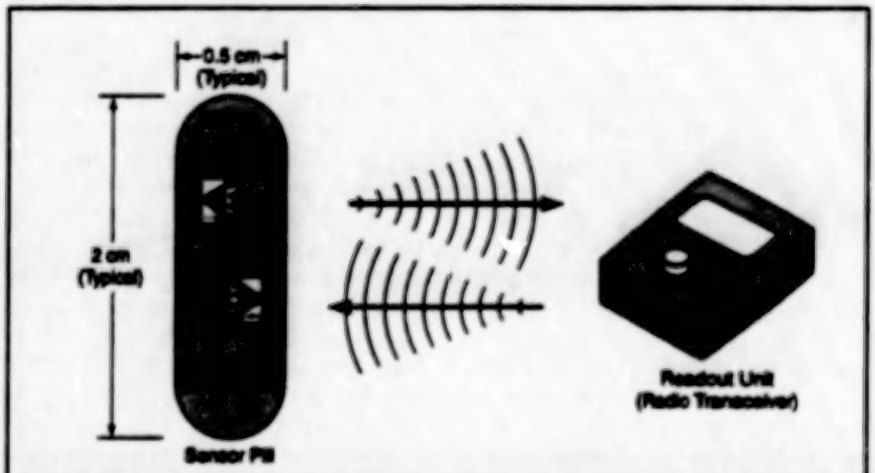

A Large Pill would contain sensors and electronic circuits for radio telemetry, and perhaps devices for local delivery of drugs. The pill would be interrogated and/or controlled by use of a hand-held radio transceiver. Recent developments in integrated circuits and microelectromechanical system would be exploited in designing and fabricating improved sensor pills.

The proposed pills would incorporate some advances beyond the commercial

units. The only sensor readings provided by the commercially available sensor pills are temperature measurements. The proposed sensors would also provide indications of the presence of blood, bacteria, and chemicals of interest. Unlike the commercial sensor pills, the proposed sensor pills would not contain batteries. A sensor pill of the proposed type would be interrogated by use of a hand-held radio transceiver, and would derive its power from a radio beam emitted by the transceiver (see figure), in the same manner as that of a sensor patch described in the preceding article.

The pH sensors would most likely be based on ion-sensitive field-effect transistors (ISFETs), integrated onto the same chips that contain the communication circuits. The temperature sensors could also be integrated onto the same chips.

The bacteria sensors would exploit surface acoustic waves on membranes coated with antigens to the species of interest (for example, H. pylori — the species that causes gastrointestinal ulcers). The bacteria of interest would either attach themselves to the antigens on the membrane or else pull the antigens off; in either case, the result would be a change in the mass of the membrane and thus a change in the acoustic resonance frequency.

Most likely, the sensory areas on a pill would be protected by a cap or by a single-use coat made of a biocompatible polymer, until the time for sensor readings. In preparation for sensor readings, a microelectromechanical actuator could remove a cap; alternatively, a polymer coat could be melted or could be torn off by a microelectromechanical actuator. In the case of an array of sensors, the polymer coat could be removed from any or all sensor(s) at the same time or at different times; thus, even if the sensors were single-use devices, it would be possible to take readings at different times.

This work was done by Gisela Lin, William Tang, and Linda Miller of Caltech and Shlomo Raz of UCLA Medical School for **NASA's Jet Propulsion Laboratory.** *Further information is contained in a TSP [see page 1].*

In accordance with Public Law 96-517, the contractor has elected to retain title to this invention. Inquiries concerning rights for its commercial use should be addressed to

Technology Reporting Office
JPL
Mail Stop 122-116
4800 Oak Grove Drive
Pasadena, CA 91109
(818) 354-2240

Refer to NPO-20652, volume and number of this NASA Tech Briefs *issue, and the page number.*

Urine-Sample-Collection Device for Use on the Space Shuttle

Lightweight design, small size, and ease of use encourage routine collection of samples.

Lyndon B. Johnson Space Center, Houston, Texas

The in-flight urine collection absorber (IUCA) is a Johnson Space Center (JSC) breakthrough. It features a lightweight, compact design and is easy to use for collection of urine samples by male and female space shuttle crewmembers. The IUCA is superior to currently available hardware for flight urine-sampling protocols that do not require measurement of sample volumes. In addition, its lightweight design makes it desirable for space flight, where weight is a prime concern. Its utility has been confirmed in tests employing stable isotopes (oxygen-18 and deuterium) conducted at JSC. These tests showed that the IUCA, which can be placed in either male or female urine-collection funnels of the shuttle-waste-collection system, outperforms the standard urine collection device (UCD). Although there is no apparent commercial use at this time, the IUCA will benefit the space program by increasing capabilities for research in life sciences research capabilities.

On shuttle missions, collection of urine by use of UCDs has typically been restricted to male crewmembers. In order to collect samples from female crewmembers, it has been necessary to add flight hardware — a urine-monitoring system. This system was infrequently manifested on flights because of its considerable size and weight. Although the UCDs typically employed on the shuttle are cumbersome and are susceptible to leakage, they continue to be used to satisfy the urine-collection requirements of many flight experiments.

While many scientific protocols require information on urine volume, experiments in which stable isotopes are used typically rely on the ratio between concentrations of two compounds in urine; hence, urine-volume data are not required. While recent modifications have improved UCD function, constraints on volume and weight of equipment carried aboard the spacecraft limit space for storage of both empty and filled UCDs, and this limitation profoundly affects missions of any duration. Thus, identifying a means of collecting small urine samples from male and female crewmembers that required minimal volume and weight became a critical concern for JSC scientists.

The IUCA addresses this concern for urine-volume-independent studies. Prototype IUCA units were developed to collect small samples during flight. Each unit has a conical shape and an area ≈75 cm². It was built from a material that is known to absorb 20.4 g of water per 100 cm² of area. Its assembly weighs ≈20 g empty and 35 g full, as compared to the UCD assembly, which weighs 65 g empty and can weigh from 300 to 500 g when full. The IUCA is placed in either a male or female urine-collection funnel of the shuttle-waste-control system (WCS). As a crewmember voids, the vortex action created by the shuttle vacuum system causes urine to saturate the IUCA. Upon completion of the void, the IUCA is removed from the WCS, placed in two zipper-locked bags, and stored in an absorber containment bag for return. The prototype was tested several times for volume recovery by use of a WCS mock-up in Building 5 at JSC. However, due to gravitational effects, results were inconclusive. Flight safety testing was completed, and the prototype units were subsequently certified for use in flight.

Preliminary studies were performed at JSC to evaluate the effect of the absorbent paper on the analysis of deuterium and oxygen-18 — two isotopes currently used to determine energy expenditure, water metabolism, and body composition in flight. Data obtained by use of the absorbent paper were identical to those obtained in sampling by use of conventional methods.

The IUCA will benefit the space program for which it was intended, where it can advance life sciences research by making it easy for all crewmembers to collect urine samples. While its compact nature assures compliance with shuttle mission requirements, its advanced design will prove equally adaptable to the International Space Station and to future long-duration space missions.

This work was done by Scott Smith and Helen Lane of **Johnson Space Center** *and Janis Davis-Street and Jeannie Nillen of Lockheed Martin Engineering & Science. Further information is contained in a TSP [see page 1].*

MSC-22748

END

03-7-00